

The Response of Quasigeostrophic Oceanic Vortices to Tropical Cyclone Forcing

BENJAMIN JAIMES AND LYNN K. SHAY

*Division of Meteorology and Physical Oceanography, Rosenstiel School of Marine and Atmospheric Science,
University of Miami, Miami, Florida*

GEORGE R. HALLIWELL

NOAA/AOML/PhOD, Miami, Florida

(Manuscript received 13 January 2011, in final form 13 May 2011)

ABSTRACT

The response of quasigeostrophic (QG) oceanic vortices to tropical cyclone (TC) forcing is investigated using an isopycnic ocean model. Idealized oceanic currents and wind fields derived from observational data acquired during Hurricane Katrina are used to initialize this model. It is found that the upwelling response is a function of the curl of wind-driven acceleration of oceanic mixed layer (OML) currents rather than a function of the wind stress curl. Upwelling (downwelling) regimes prevail under the TC's eye as it translates over cyclonic (anticyclonic) QG vortices. OML cooling of $\sim 1^{\circ}\text{C}$ occurs over anticyclones because of the combined effects of downwelling, instantaneous turbulent entrainment over the deep warm water column (weak stratification), and vertical dispersion of near-inertial energy. By contrast, OML cooling of $\sim 4^{\circ}\text{C}$ occurs over cyclones due to the combined effects of upwelling, instantaneous turbulent entrainment over regions of tight vertical thermal gradients (strong stratification), and trapping of near-inertial energy that enhances vertical shear and mixing at the OML base. The rotational rate of the QG vortex affects the dispersion of near-inertial waves. As rotation is increased in both cyclones and anticyclones, the near-inertial response is shifted toward more energetic frequencies that enhance vertical shear and mixing. TC-induced temperature anomalies in QG vortices propagate westward with time, deforming the cold wake. Therefore, to accurately simulate the impact of TC-induced OML cooling and feedback mechanisms on storm intensity, coupled ocean-atmosphere TC models must resolve geostrophic ocean eddy location as well as thermal, density, and velocity structures.

1. Introduction

Upper-ocean thermal structures encountered by tropical cyclones (TC) are seldom uniform. These storms usually move over energetic, deep, warm western boundary currents and warm- and cold-core geostrophic eddies (WCEs and CCEs, respectively; Fig. 1), where horizontal thermal gradients tighten over distances of $O(10)$ km. Starting with the studies of Leipper (1967) and Shay et al. (1992), the presence of geostrophic oceanic features has been shown to impact the efficiency of TCs to cool the oceanic mixed layer (OML), modulating sea surface temperature (SST) cooling and the ensuing air-sea

fluxes into the TC (i.e., negative feedback; Chang and Anthes 1978). In warm oceanic geostrophic features, OMLs are deep and the associated ocean heat content values relative to the 26°C isotherm depth often exceed 100 kJ cm^{-2} . Reduced OML cooling response has been observed in these warm features, thereby providing a sustained heat flux that, under neutral to favorable atmospheric conditions (e.g., weak atmospheric shear), contributes to rapid TC intensification (Jacob et al. 2000; Shay et al. 2000; Jacob and Shay 2003; Lin et al. 2005; Shay and Uhlhorn 2008; Wada and Chan 2008; Jaimes and Shay 2009, hereafter JS09; Shay 2009). Numerical models have reproduced this positive impact of high oceanic heat content and reduced cooling on TC intensification (Schade and Emanuel 1999; Hong et al. 2000; Lin et al. 2005; Wu et al. 2007). By contrast, shallow OMLs, less ocean heat content, and more vigorous OML cooling response in CCEs may contribute to rapid TC weakening (Walker et al. 2005; Halliwell

Corresponding author address: Benjamin Jaimes, Division of Meteorology and Physical Oceanography, Rosenstiel School of Marine and Atmospheric Science, University of Miami, 4600 Rickenbacker Causeway, Miami, FL 33149-1098.
E-mail: bjaimes@rsmas.miami.edu

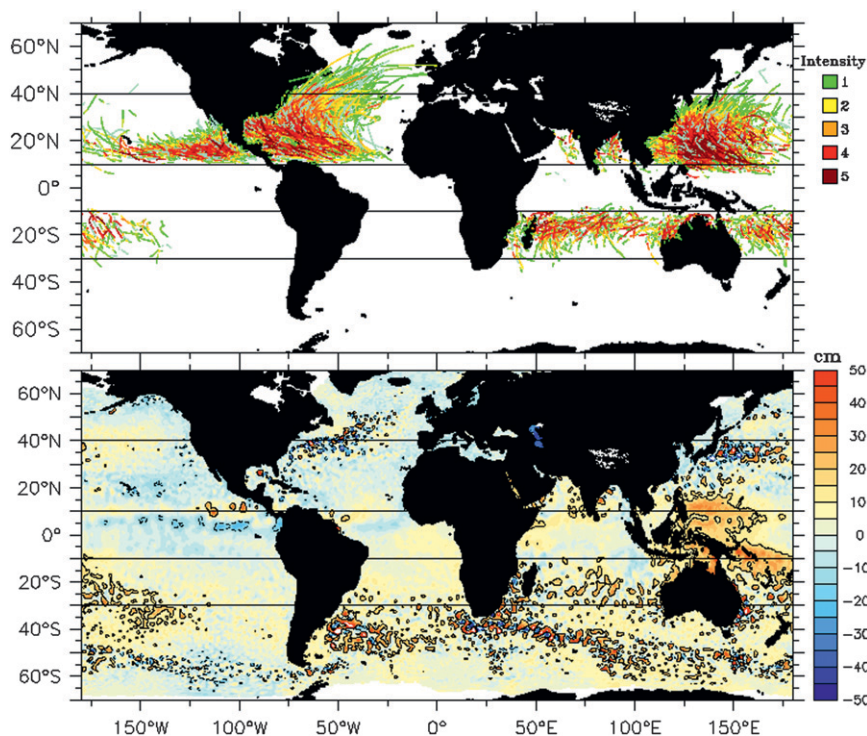


FIG. 1. (top) Distribution of all tropical cyclone trajectories on record (hurricane intensity level), from the National Hurricane Center and Joint Typhoon Warning Center databases; trajectory segments with higher storm intensity level are on top. (bottom) Typical global distribution of sea surface height anomaly (SHA), from a daily composite of the Archiving, Validation, and Interpretation of Satellite Oceanographic data (AVISO) product. Blue (red) shades are for cyclonic (anticyclonic) ocean eddies; contours are for $\text{SHA} = \pm 15$ cm.

et al. 2008; JS09). Understanding this contrasting OML thermal response of geostrophic oceanic features to wind stress forcing is thus important for predicting accurate TC intensity changes in coupled numerical models.

Recent numerical studies differentiated the OML thermal response of warm oceanic features and a quiescent ocean to TC wind forcing for various OML turbulence closures (Jacob and Shay 2003). Realistic simulations of the ocean response to Hurricane Ivan (2004) illustrated the critical importance of correctly initializing WCEs and CCEs to correctly simulate the contrasting magnitude and pattern of SST cooling (Halliwell et al. 2008, 2011). A unique dataset acquired in the Gulf of Mexico during TCs Katrina and Rita (Rogers et al. 2006; JS09; Shay 2009) allowed assessment of the contrasting OML cooling response of WCEs and CCEs to major TCs, during the forced stage (relatively short time scale when the TC is overhead) and relaxation stage in the wake of the storm [formally a geostrophic adjustment process where near-inertial oscillations (NIOs) propagate away from the storm track; Gill 1984; Shay et al. 1989, 1990]. Based on these observational data and a theoretical model (Stern

1965), JS09 hypothesized that contrasting OML cooling levels can develop over geostrophically balanced eddies because the upwelling response is a function of the underlying geostrophic relative vorticity ζ_g . Upwelling (downwelling) regimes were predicted to predominantly develop in regions where the wind stress vector is with (against) geostrophic OML currents (JS09). The impact of ζ_g extended to the relaxation stage: contrasting NIO dispersion was found to be a function of ζ_g that affected the distribution of momentum, vertical shear, and mixing in the upper ocean. The OML cooling response was reduced over regions of anticyclonic ζ_g , as near-inertial shear instability vanished because NIOs rapidly propagated into the thermocline. By contrast, cooling induced by vertical mixing was intense over regions of cyclonic ζ_g because NIOs were trapped in OMLs that increased vertical shear instability at the layer base (Jaimes and Shay 2010, hereafter JS10).

Several important issues are still open. First, pertaining to the TC-driven upwelling is whether the upwelling/downwelling response inside CCEs/WCEs is affected by the angle of approach of the storm to the geostrophic vortex, because this would impact the projection of the

wind stress vector on the prestorm OML velocity vector. In association with near-inertial current shear-driven cooling, another question is whether the rotational constraints in geostrophic vortices can impact the vertical structure of forced baroclinic modes and shear-driven mixing in the wake of TCs (Shay et al. 1989). The impact of the relative vorticity of mesoscale features (e.g., Kunze 1985; Danioux et al. 2008) and geostrophic kinetic energy (Young and Ben Jelloul 1997) on the structure of baroclinic modes and the vertical propagation of near-inertial energy were earlier explained, but the effect of differing rotational rates of the wave-supporting medium (geostrophic vortex) on near-inertial shear-driven mixing in the wake of TCs still needs to be resolved. Another aspect of the near-inertial current response to TC forcing considers the spatial structure of the cold wake of TCs over geostrophic oceanic features. In quiescent ocean regimes, the cold wake usually extends over a distance of $O(10^3)$ km and the maximum response is displaced to the right side of the storm track because of vertical shear-induced mixing or asymmetries in the surface wind field due to storm speed (Chang and Anthes 1978; Price 1981; Greatbatch 1984). However, after the passage of TCs Hilda (Leipper 1967), Ivan (Walker et al. 2005; Halliwell et al. 2008, 2011), and Katrina and Rita (JS10) over the Gulf of Mexico's CCEs, the larger TC-induced cooling levels were measured on the left side of the storm's track a few days after storm passage, which suggests that the internal wave wake of these TCs was trapped and advected by westward-propagating geostrophic CCEs.

To address these issues, aspects of the ocean response to TCs—generally well understood under quiescent ocean conditions—are investigated here with a series of numerical experiments initialized with cyclonic and anticyclonic oceanic quasigeostrophic (QG) vortices. Ocean model, wind forcing, and experimental approach are described in section 2. Using measurements acquired during TCs Katrina and Rita as the ground truth, the interest is on QG WCEs and CCEs with Rossby number (Ro) ranges characteristic of the Gulf of Mexico ($Ro < 0.1$). The TC-induced upwelling response in a QG vortex is addressed in section 3. The deepening of the OML by the wind-driven frictional velocity during the forced stage and OML deepening induced by vertical shear instability during the relaxation stage are assessed in section 4 [Jacob and Shay (2003) investigated TC-induced OML deepening in a geostrophic anticyclone; here we consider OML deepening in QG cyclones and anticyclones]. In section 5, the near-inertial velocity response is isolated in these differing vortices. Results are discussed in section 6, followed by a summary with concluding remarks in section 7.

2. Ocean model

Given that vertical entrainment is an important aspect of the problem investigated here, an isopycnic ocean model [Miami Isopycnic Coordinate Ocean Model (MICOM)] is used to reduce spurious vertical mixing. Isopycnic coordinate models suppress the spurious numerical diapycnal dispersion of material and thermodynamic properties. This allows MICOM to preserve its water mass characteristics and prevents warming of deep-water mass that has been shown to occur in models framed in Cartesian coordinates (Griffies et al. 2000). MICOM consists of four prognostic equations for the horizontal velocity vector, mass continuity, or layer thickness tendency and two conservative equations for salt and heat (Bleck and Chassignet 1994). A non-isopycnic mixed layer forms the top layer of the model.

A modified version of MICOM (Herbette et al. 2003; Morel et al. 2006; Chérubin et al. 2006) is used to include a fourth-order scheme for the nonlinear advective terms in the momentum equations and biharmonic horizontal diffusion. This modified version reduces numerical noise associated with dispersive effects and the development of shocks in frontal regimes (Morel et al. 2006). The model approach is as follows:

- 1) Buoyancy fluxes are ignored both in the density equation and in the turbulent kinetic energy (TKE) equation (for consistency) because the interest is to isolate the OML response due to internal oceanic processes, which have been proven to drive most of the TC-induced OML cooling (Price 1981; Greatbatch 1984; Shay et al. 1992, 2000; Hong et al. 2000; Jacob et al. 2000).
- 2) The turbulence closure for the OML only considers (i) instantaneous wind erosion by the wind-driven frictional velocity $w_* = (\tau/\rho_0)^{1/2}$ (Kraus and Turner 1967) and (ii) TKE production by vertical shear instability at the OML base and over the stratified ocean below (Price et al. 1986). These turbulence closures were chosen because of their mathematical simplicity and because they provide direct physical insight on important mixing process observed over the thermocline inside a CCE impacted by Katrina (JS09; JS10).
- 3) Idealized vortices (WCEs and CCEs) are initialized with an analytical model and density structures from direct measurements obtained during Katrina and Rita; these vortices satisfy the QG approximation (section 2b).
- 4) An f plane is used to prevent self-propagation of the QG vortices, which facilitates analyzing the near-inertial response at fixed points inside the stationary vortex. This approach cancels horizontal dispersion

TABLE 1. Characteristics of geostrophic features in the Gulf of Mexico. The LC is an anticyclonic feature.

Parameter	Obs		Modeled			
	LC/WCE	CCE	WCE1	WCE2	CCE1	CCE2
U (m s ⁻¹)	1–2	0.5–0.8	0.95	1.5	0.6	0.8
L (km)	200–400	100–150	250	300	150	150
OML (m)	~80	~30	~65	~80	~30	~25
Ro (U/fL)	0.05–0.1	0.05–0.08	0.06	0.08	0.06	0.08

of NIOs by meridional gradients in planetary vorticity (Gill 1984). Any resulting horizontal wave dispersion is purely driven by ζ_g .

a. Numerical domain

The computational domain is a 2000 km \times 2000 km square ocean with an initially circular QG vortex (CCE or WCE) of \sim 150–300 km in diameter located at the center; these horizontal scales are representative of Gulf of Mexico's CCEs and WCEs (Table 1). The central latitude of the domain is 26.9°N, which allows the reproduction of near-inertial responses at the latitude of moorings used in JS09 and JS10. The horizontal grid resolution is 10 km, allowing the resolution of horizontal wavelengths larger than 20 km, which is adequate for resolving CCEs and WCEs and is also adequate to resolve the basic eye and eyewall structure in the atmospheric forcing fields (Halliwell et al. 2011). The bottom is flat, and lateral boundary conditions are closed.

Three vertical resolutions were used: 12, 23, and 47 layers (Fig. 2). In every case, the model's top layer is the OML, and, with the exception of an initially quiescent isopycnic bottom layer of 4000 m in thickness, the rest of the layers represent the QG vortex. The thickness of both the OML and isopycnal layers—and so the vortex's vertical length—is determined by the analytical model (section 2b) as a function of the radius of the vortex, the target maximum azimuthal velocity, and the realistic background stratifications presented in Fig. 2. For a given WCE/CCE, the initial OML thickness is nearly the same for every vertical resolution. Given that experiments with higher vertical resolution improve the representation of the stratified ocean below the OML, OML cooling, and vertical dispersion of near-inertial energy, the discussion focuses on the 47-layer numerical experiments that have vertical resolution of 10 m between the OML and the thermocline, allowing the model to resolve vertical wavelengths larger than 20 m. (The vertical sampling grid in the moorings used in JS09 and JS10 is \sim 8 m.)

b. Analytical model

The model vortex is constructed by introducing a potential vorticity anomaly (PVA) in a stack of initially

unperturbed isopycnic layers (Fig. 2). The layer's PVA is the departure from ambient potential vorticity and is defined by the quantity (Morel and McWilliams 2001; Herbertte et al. 2003; Morel and Thomas 2009)

$$\begin{aligned} \text{PVA}_k &= H_k \left(\frac{\zeta_g + f}{h_k} - \frac{f}{H_k} \right) \\ &= \frac{H_k}{h_k} \left[\zeta_g - \frac{f(h_k - H_k)}{H_k} \right], \end{aligned}$$

where k is a layer index, f/H_k is ambient potential vorticity on the assumed f plane, h_k is instantaneous layer thickness, and H_k is constant and represents the unperturbed layer thickness (Fig. 2). Note that PVA has units of vorticity, its value at rest is zero, and because it is a linear function of potential vorticity $PV = (\zeta_g + f)/h_k$ it has the same properties of Lagrangian conservation (Morel and Thomas 2009).

An initial PVA profile is defined that satisfies the QG approximation and the condition that the vortex is isolated (the area integral of ζ_g vanishes at all depths; Flierl 1987). In the case of Gulf of Mexico's WCEs and CCEs from MICOM simulations, these conditions are fulfilled by using a continuous-power exponential radial profile and annular shielding in the PVA for the isopycnic layers above 700-m depth (Chérubin et al. 2006),

$$\text{PVA}_k = \Delta Q_k \left[1 - \frac{\alpha}{2} \left(\frac{r}{R} \right)^\alpha \right] \exp \left[- \left(\frac{r}{R} \right)^\alpha \right], \quad (1)$$

and a power exponential radial profile for isopycnic layers extending between the 700- and 950-m depths where the annular shielding vanishes (L. Chérubin 2011, personal communication),

$$\text{PVA}_k = \Delta Q_k \exp \left[- \left(\frac{r}{R} \right)^\alpha \right], \quad (2)$$

where $\text{PVA}_k = 0$ in the bottom layer, ΔQ_k is the maximum PVA in layer k and measures the vortex strength, R is the vortex radius, r the radial distance from the vortex's center, and the parameter α determines the width of the vortex shield (i.e., the horizontal shear at

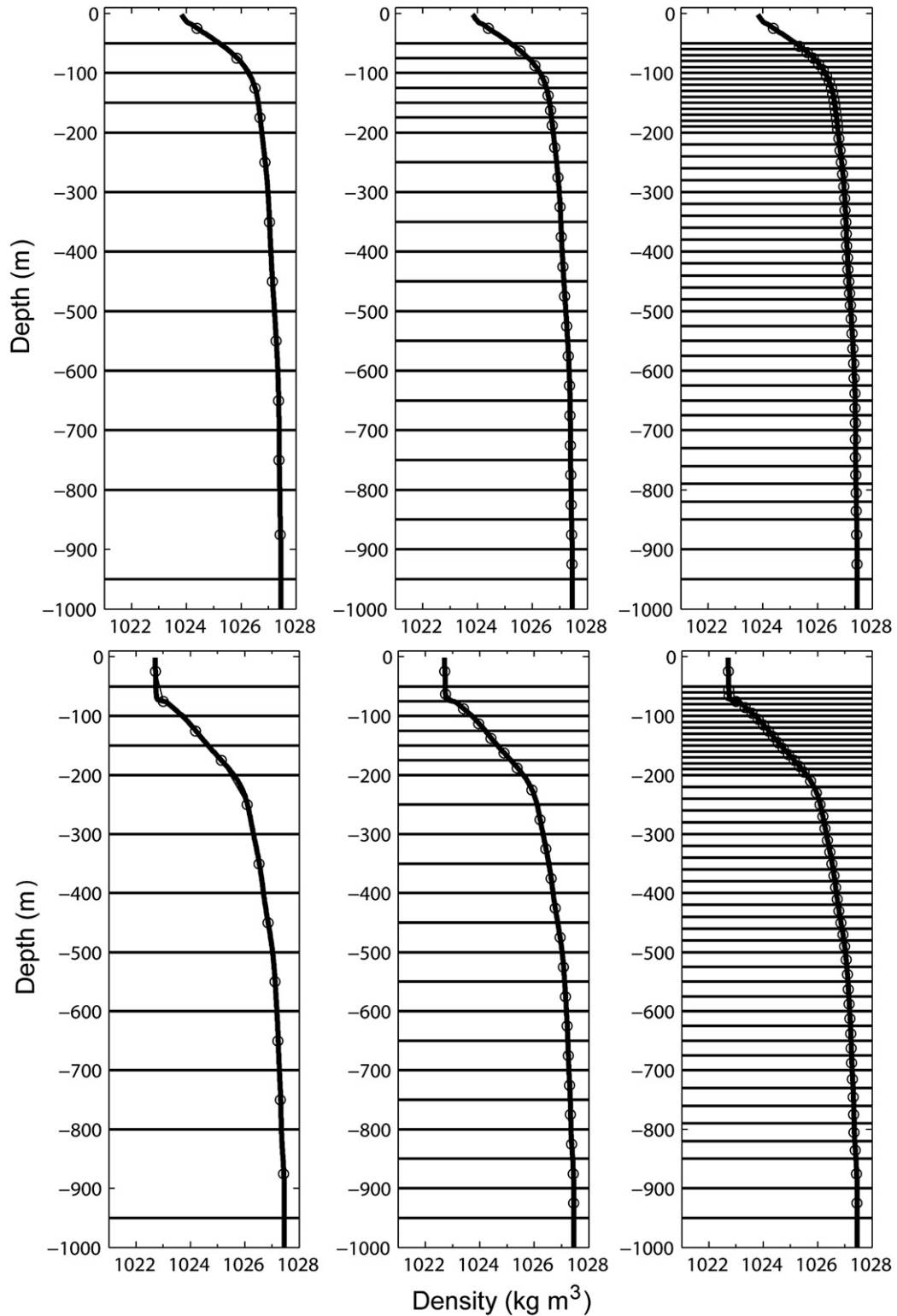


FIG. 2. Initial background stratification used in experiments with (left to right) 12, 23, and 47 isopycnic layers for (top) CCEs and (bottom) WCEs. The QG vortex is constructed by introducing a PV anomaly [Eqs. (1) and (2)] into these unperturbed background stratifications. The circles represent the background model density, and the bold line is the observed density profile (smoothed via polynomial fit). The horizontal lines represent the initial layer thickness outside the QG vortex. The top layer is the OML, and the bottom layer is not shown.

the vortex boundaries). These profiles ensure that (i) the vortex is stable and (ii) the total circulation is zero for any α in each layer (Carton and Legras 1994). For fixed α and R , ΔQ_k is determined so that the set of Eqs. (1) and (2) reproduces, via potential vorticity inversion, the maximum vortex azimuthal speed observed in WCEs and CCEs. Background stratification in the idealized vortex is defined from density fields derived from pre-Rita observational data (JS09).

c. Wind forcing

To keep the numerical experimentation as simple yet as realistic as possible, the ocean model is forced with idealized wind fields derived from the H*Wind product produced by the National Oceanic and Atmospheric Administration's Hurricane Research Division (http://www.aoml.noaa.gov/hrd/data_sub/wind.html). The wind field of TC Katrina at maximum intensity over the Loop Current (LC) system is used (category-5 hurricane at 2230 UTC 28 August 2005; JS09). Based on this snapshot, constant wind fields were derived with a drag coefficient C_d computed from the Large and Pond (1981) relationship but capped at maximum value of 2.6×10^{-3} based on recent results indicating a saturation value of C_d between 27 and 35 m s^{-1} wind speeds (Powell et al. 2003; Donelan et al. 2004; Shay and Jacob 2006; French et al. 2007; Vickery et al. 2009). The saturation level of C_d is set at a wind speed of 27 m s^{-1} . The storm moves along a straight track at an angle of 45° from true north (Fig. 3). Katrina and Rita propagated at an angle of 33.7° and 63.4° from true north over the Loop Current system, respectively. Using a realistic, constant translation speed of Katrina of 6.3 m s^{-1} , wind fields were constructed at 30-min intervals along the storm track. Linear interpolation from these 30-min wind fields is used to force the model every baroclinic time step (180 s).

d. Experiments

Based on observed characteristics of Gulf of Mexico's WCEs and CCEs, four QG vortices are reproduced (Table 1 and Fig. 4): WCE1 ($\text{Ro} = 0.06$), WCE2 ($\text{Ro} = 0.08$), CCE1 ($\text{Ro} = 0.06$), and CCE2 ($\text{Ro} = 0.08$). These vortices are initialized in model runs with parameters summarized in Table 2. After introducing the corresponding PV anomaly in every layer via Eqs. (1) and (2), the initial vertical length of WCE1, WCE2, CCE1, and CCE2 is approximately 1270, 1350, 700, and 610 m, respectively (Fig. 4e). These values are consistent with vertical scales reported for Gulf of Mexico's WCEs (>1200 m; Elliot 1982) and CCEs (Hamilton 1992) based on direct measurements. The model initial OML thicknesses (Table 1 and Figs. 4a–d) are comparable to observed values during Hurricanes Katrina and Rita

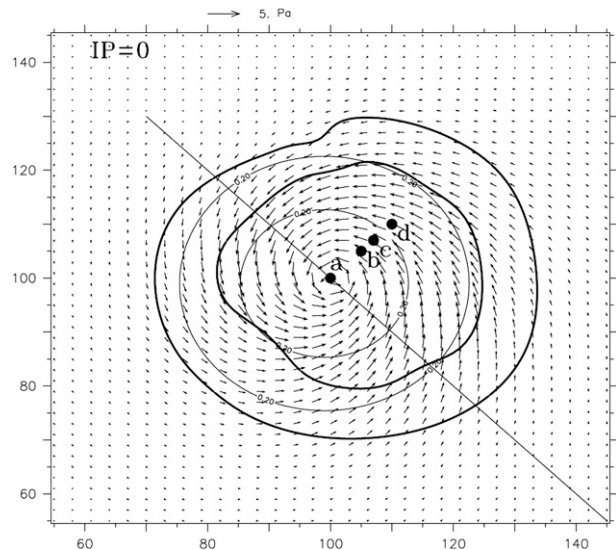


FIG. 3. Constant wind field used to force the ocean model (from the H*Wind product). Vectors are wind stress calculated with a drag coefficient capped at a standard 10-m wind speed of 27 m s^{-1} (saturation level in the present treatment). External and inner bold contours are for tropical storm winds (20 m s^{-1}) and winds at saturation level, respectively. The straight line is the storm track. The large and small thin circles are 0.2 m s^{-1} contours of prestorm OML currents for model WCEs and CCEs, respectively. Here, IP = 0 represents the time when the storm's eye is over the WCE's/CCE's center. Black dots are model moorings on the cross-track direction.

(Fig. 1.2 of Jaimes 2009). The main focus is on CCE2 and WCE1, because these model vortices are similar to eddy features that interacted with Katrina (CCE) and Rita (Loop Current bulge).

3. TC-induced upwelling in a QG vortex

Under quiescent ocean conditions, wind-driven horizontal current divergence produces a shallow OML under the TC's center and a deeper OML outside the center. Upwelling of cold thermocline water compensates this horizontal flow divergence under the storm's eye. The region of maximum upwelling is confined to within twice the radius of maximum wind stress (O'Brien and Reid 1967; O'Brien 1967). By considering a standard 10-m wind speed $U_{10} = 27 \text{ m s}^{-1}$ (assumed saturation level of the drag coefficient in the present treatment), drag coefficient $C_d = 2.6 \times 10^{-3}$ (Powell et al. 2003), air density $\rho_a = 1.2 \text{ kg m}^{-3}$, seawater density $\rho_0 = 1025 \text{ kg m}^{-3}$, OML thickness $h = 45 \text{ m}$ (typical value away from eddies in the Gulf of Mexico), and a latitude of 27°N ($f \sim 6.62 \times 10^{-3} \text{ s}^{-1}$), the Ekman current $u_e \cong \tau / \rho_0 f h$ (where $\tau = \rho_a C_d U_{10}^2$) that one could expect is $\sim 0.75 \text{ m s}^{-1}$, which is comparable to OML geostrophic

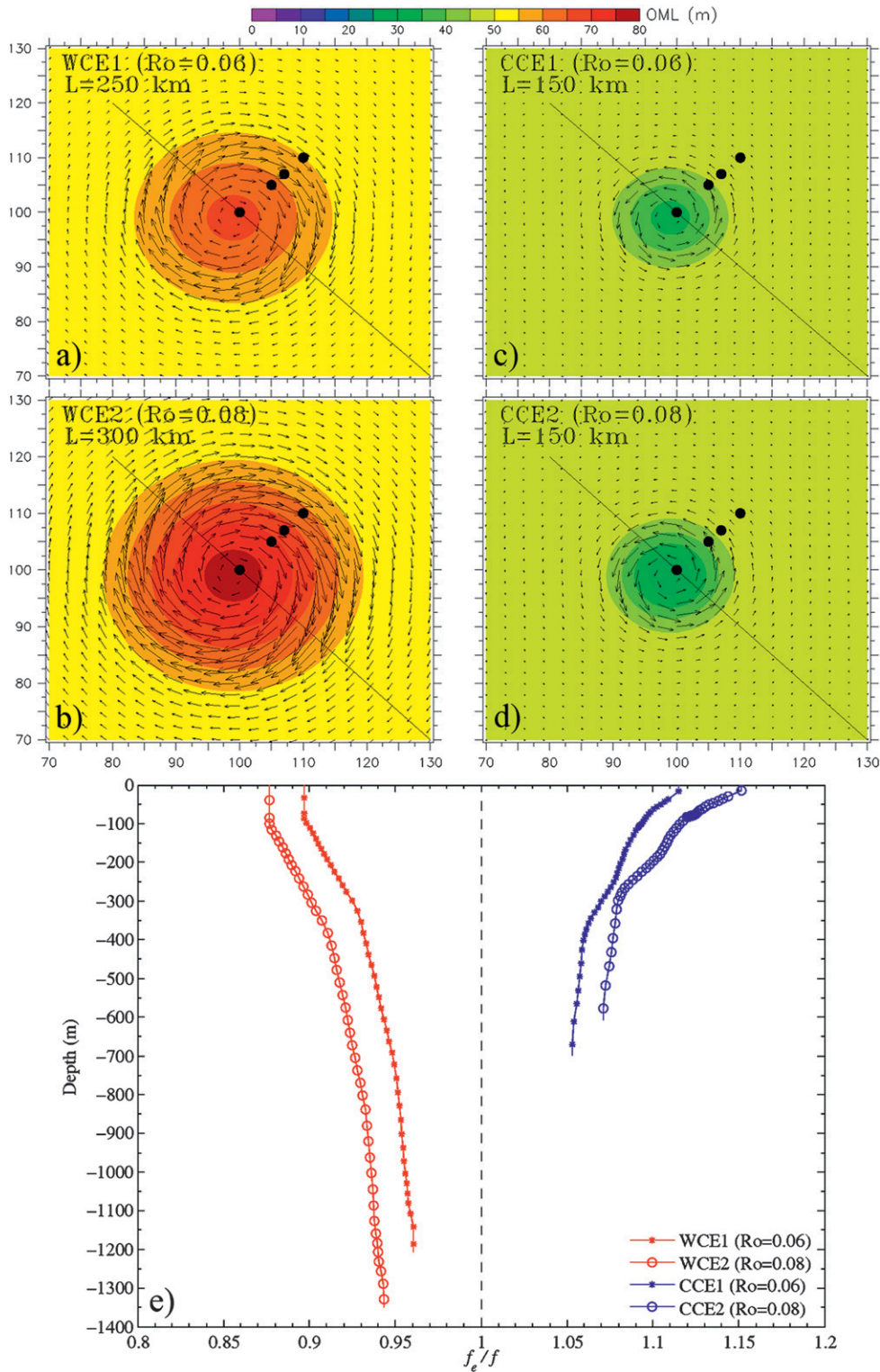


FIG. 4. Initial conditions of the four types of model vortices: (a) WCE1, (b) WCE2, (c) CCE1, and (d) CCE2. Color is the initial OML thickness, vectors are OML geostrophic currents, the black line is the storm track, L is the vortex's radius, and black dots are model moorings on the cross-track direction. (e) Initial vertical length of the QG vortices based on the vertical structure of the effective Coriolis parameter $f_e = f + \zeta_g/2$ (Kunze 1985) normalized by f at the vortex's center, where ζ_g is geostrophic relative vorticity. In (e), the top 46 isopycnal layers are shown, and the symbols represent the depth of the layer's center after introducing the PV anomaly [Eqs. (1) and (2)] into the initially unperturbed stratifications presented in Fig. 2.

TABLE 2. List of experiments. The symbol ρ indicates the type of density field used to initialize the ocean model (GCW stands for Gulf Common Water and represents EFO conditions). KT and PWP stand for the Kraus–Turner and Price–Weller–Pinkel turbulence closures for the OML, respectively. Here, β indicates β plane. Control experiments are in italic bold, and changed parameters are in bold. Here, R_c is the critical limit for both bulk and gradient Richardson numbers, and ΔQ_k is maximum PVA.

WCE										
Expt	ΔQ_k ($\times 10^{-5}$) s $^{-1}$	Vortex	ρ	U m s $^{-1}$	L km	Ro	KT	PWP	R_c	β ($\times 10^{-11}$) s $^{-1}$ m $^{-1}$
<i>wce1_01</i>	-5.77	WCE1	WCE	0.95	250	0.06	—	—	—	0
wce1_04	-5.77	WCE1	WCE	0.95	250	0.06	Yes	—	—	0
wce1_05	-5.77	WCE1	WCE	0.95	250	0.06	Yes	Yes	1	0
wce1_06	-5.77	WCE1	WCE	0.95	250	0.06	Yes	Yes	0.65	0
wce2_01	-8.50	WCE2	WCE	1.50	300	0.08	—	—	—	0
wce2_02	-8.50	WCE2	WCE	1.50	300	0.08	Yes	—	—	0
wce2_03	-8.50	WCE2	WCE	1.50	300	0.08	Yes	Yes	1	0
EFO										
Expt	ΔQ_k	Vortex	ρ	U	L	Ro	KT	PWP	R_c	β
<i>efo1_01</i>	0	—	GCW	0	0	0	—	—	—	0
efo1_02	0	—	GCW	0	0	0	Yes	—	—	0
efo1_03	0	—	GCW	0	0	0	Yes	Yes	1	0
CCE										
Expt	ΔQ_k	Vortex	ρ	U	L	Ro	KT	PWP	R_c	β
<i>cce1_01</i>	6.05	CCE1	CCE	0.6	150	0.06	—	—	—	0
cce1_04	6.05	CCE1	CCE	0.6	150	0.06	Yes	—	—	0
cce1_05	6.05	CCE1	CCE	0.6	150	0.06	Yes	Yes	1	0
cce1_06	6.05	CCE1	CCE	0.6	150	0.06	Yes	Yes	1	2.04
cce2_01	8.17	CCE2	CCE	0.8	150	0.08	—	—	—	0
cce2_02	8.17	CCE2	CCE	0.8	150	0.08	Yes	—	—	0
cce2_03	8.17	CCE2	CCE	0.8	150	0.08	Yes	Yes	1	0
cce2_04	8.17	CCE2	CCE	0.8	150	0.08	Yes	Yes	1	2.04
cce2_05	8.17	CCE2	CCE	0.8	150	0.08	Yes	Yes	0.65	0
cce2_06	8.17	CCE2	CCE	0.8	150	0.08	—	—	—	2.04

currents in CCEs (Table 1) and smaller than OML geostrophic currents in WCEs and western boundary currents (1–2 m s $^{-1}$). Under strong background flow conditions, the prestorm surface currents can instantaneously influence wind-driven frictional OML currents. Observational evidence (JS09) and theoretical arguments (Stern 1965) suggest that the upwelling response is a function of the underlying OML geostrophic flow. This should be an expected result, because the wind stress and OML geostrophic currents are vectors that interact with each other. The upwelling velocity $w = (\mathbf{k} \times \boldsymbol{\tau} / \rho_0 f^2) \cdot \nabla \zeta_g$ predicted by Stern's (1965) theory in a QG vortex resembles classical Ekman pumping. However, it is not associated with the wind stress curl but with the curl of wind-driven current acceleration along isopycnal surfaces when the vertical position of these surfaces varies in geostrophically balanced features.

To address this hypothesis, a series of numerical experiments are presented in which the same wind stress is applied on WCEs, CCEs, and eddy-free ocean (EFO)

conditions [i.e., initially quiescent ocean and stratification from Gulf Common Water (GCW)]. The approach is to neglect vertical entrainment velocities across the OML base (no turbulence closure for the OML) so that changes in OML thickness are produced only by horizontal current divergence. Mathematically, this assumption is represented as following. For rather direct physical insight, the discussion focuses on OML bulk models, which are based on the density and momentum equations, given by

$$\frac{\partial \rho}{\partial t} = \frac{B}{\rho_0 g h} + \frac{\delta \rho}{h} \frac{\partial h}{\partial t} \quad \text{and} \quad (3)$$

$$\frac{\partial \mathbf{v}}{\partial t} = -\mathbf{k} \times (f\mathbf{v}) + \frac{\boldsymbol{\tau}}{h\rho_0} + \frac{\delta \mathbf{v}}{h} \frac{\partial h}{\partial t}, \quad (4)$$

respectively, where $B = g\rho_0[\alpha_0 Q_0 + \beta_0 S(E - P)]$ is the air–sea buoyancy flux, $E - P$ is evaporation minus precipitation, h is OML thickness, and the rest of the

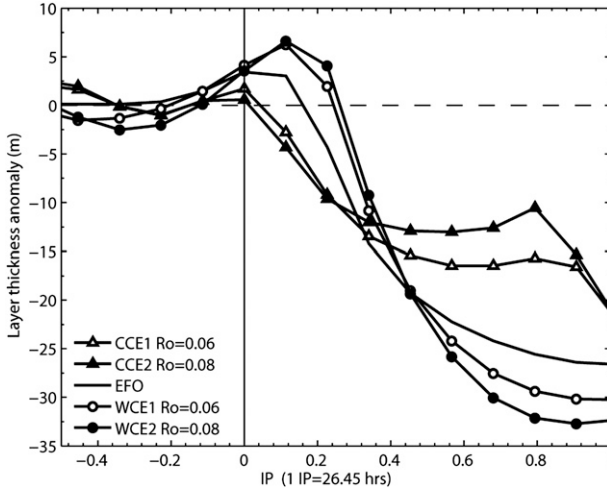


FIG. 5. Evolution of layer thickness anomaly η by horizontal current divergence in the top layer of the ocean model at mooring a (see Fig. 3), where $\eta(\text{IP}) = h(\text{IP}) - h(\text{IP} = -1.5)$ and h is the instantaneous OML thickness. Mooring a was under the storm's eye approximately from $\text{IP} = -0.25$ to $\text{IP} = 0.25$. The model initial state corresponds to $\text{IP} = -1.5$.

notation is conventional. Notice that the first term on the right-hand side of Eq. (3) is ignored in the present treatment. The additional equation to close the system is (Niiler and Kraus 1975)

$$\frac{\partial h}{\partial t} = -\nabla \cdot (\mathbf{v}h) - w_e, \quad (5)$$

where w_e is the vertical entrainment velocity, which will be discussed in section 4a but is neglected here. Therefore, the OML thickness is governed by horizontal current divergence,

$$\frac{\partial h}{\partial t} = -\nabla \cdot (\mathbf{v}h),$$

where τ is the only source according to Eq. (4).

As shown in Fig. 5, for the same wind forcing, wind-driven horizontal current divergence is a function of the underlying geostrophic flow, as suggested by direct observations (JS09) and theoretical predictions (Stern 1965). Notice that Ro has negligible influence on the upwelling response during the first quarter of the inertial period (IP) and becomes more important afterward (relaxation stage), impacting near-inertial pumping and the coupling of the OML with the thermocline. In the EFO case, the amplitude of the upwelling response exhibits intermediate levels compared with WCEs and CCEs.

Outside the QG vortex, the vertical velocity response reproduces the classical pattern, where the region of minimum OML thickness extends under the storm's eye and within $2R_{\text{max}}$ (R_{max} is the radius of maximum winds)

and the OML is deeper outside this region (Fig. 6). However, a dipole in the vertical velocity emerges in the vortex's interior, in both WCEs and CCEs. Downwelling development under the storm's eye in WCEs is striking (Figs. 6a–c). Regions of maximum upwelling/downwelling extend along streamlines of maximum azimuthal geostrophic velocity, in both WCEs and CCEs. By shifting the storm track westward, this region of maximum upwelling/downwelling moves radially toward more energetic geostrophic streamlines, because the inner vortex region becomes influenced by stronger winds (cf. regions of maximum downwelling in Figs. 6d–f at the second mooring from left to right). In terms of horizontal extension, upwelling (downwelling) regimes predominate inside CCEs (WCEs). However, the confined counterpart vertical velocity is stronger and the area integral of the vertical velocity nearly vanishes over the OML, which satisfy mass conservation principles in the vortex's interior, in both WCEs and CCEs.

Morel and Thomas (2009) evaluated Stern's (1965) theory in a series of numerical experiments; they found that the dipole in the vertical velocity emerges in QG vortices even when these features are influenced by a uniform wind stress with no curl. In these experiments (and so in Stern's theory), the curl of wind-driven acceleration of geostrophic currents drives the dipole. This curl emerges where the initial OML thickness is not uniform (as in WCEs and CCEs). Under these circumstances, the strong gradient of geostrophic vorticity acts like a beta effect that creates secondary potential vorticity anomalies in the inner vortex region. Differential advection of geostrophic vorticity by the wind stress is the mechanism that creates the dipole or beta gyres (Morel and Thomas 2009).

4. OML deepening

To reproduce more realistic OML thicknesses, now we use the full version of Eq. (5) that considers OML deepening by the vertical entrainment velocity w_e .

a. Entrainment model

The vertical entrainment velocity w_e at the OML base is calculated with a turbulence closure based in the model of Niiler and Kraus (1975). In this closure, it is assumed that the rate of TKE production less dissipation equals the rate of work done by turbulence against buoyancy. By neglecting air–sea fluxes (i.e., adiabatic ocean), the steady-state balance obtained by vertical integration of the TKE equation over the OML is (parameterized form)

$$g \frac{\delta \rho}{\rho_0} \frac{h}{2} w_e = m_1 w_*^3 + m_2 w_e \frac{\delta \mathbf{v}^2}{2}, \quad (6)$$

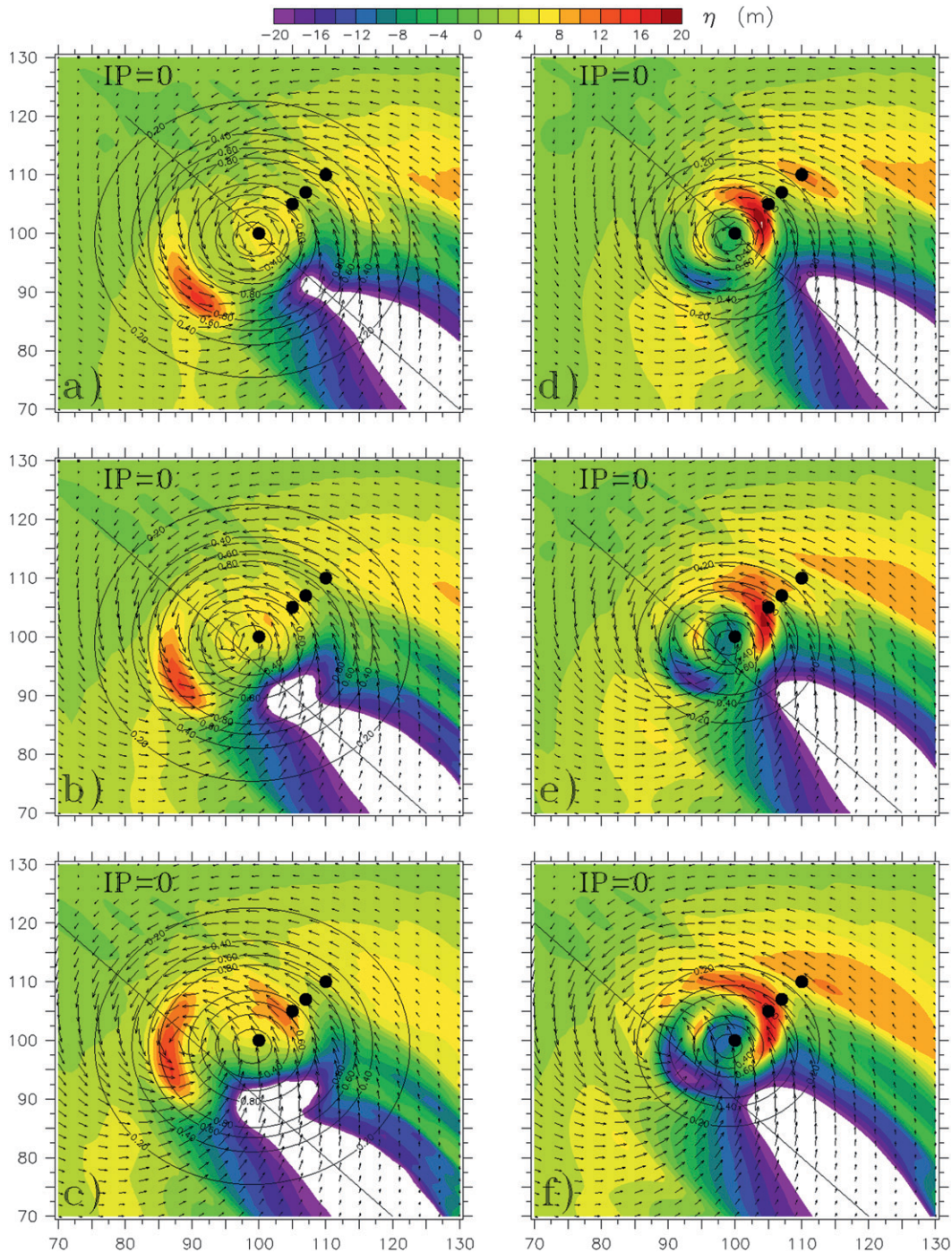


FIG. 6. OML thickness anomaly η by horizontal current divergence in (left) WCE1 and (right) CCE2, where $\eta = h(\text{IP} = 3) - h(\text{IP} = -1.5)$ and h is the instantaneous OML thickness. (b),(e) The storm track is shifted 0.5° to the west, and (c),(f) the track shifting is 1° . Circular contours are the initial magnitude of OML geostrophic currents; the contour interval is 0.2 m s^{-1} . The values of η are between -20 and -35 m in blanked regions. Vectors are for wind stress.

where the term on the left-hand side is the rate of potential energy increase caused by entrainment processes, $m_1 w_*^3$ is instantaneous turbulence production by the wind-driven OML frictional velocity [$w_* = (\tau/\rho_0)^{1/2}$],

and the second term on the right-hand side is turbulence production by vertical shear instability of horizontal currents. Empirical parameters m_1 and m_2 represent the mixing efficiency of the entrainment sources. A common

practice in bulk OML models is to set $m_2 = R_b = (g'h/\delta v^2) = 1$ as a critical stability criterion, where R_b is the bulk Richardson number, g' is reduced gravity computed at the OML base, h is OML thickness, and δv is the vertical shear of horizontal currents at the OML base. Under this assumption, there will be no entrainment at subcritical ($R_b > 1$); however, there will be so much at supercritical ($R_b < 1$) that an adjustment back to critical is forced.

Integration of Eq. (6) for a time step Δt gives

$$w_e g \frac{\delta \rho}{\rho_0} h \Delta t = \Delta t (E_1 + E_2), \quad (7)$$

where $E_1 = 2m_1 w_*^3$ and $E_2 = 5 \times 10^{-4} R_b^{-4} \delta v g' h$ is the parametric form of the vertical shear term of Eq. (6), which was derived from laboratory experiments valid for $R_b \leq 1$ (Price et al. 1978). For cases where OML deepening involves mixing over the stratified ocean below the layer, the model of Price et al. (1986) is more convenient to represent E_2 . In this model, vertical shear mixing occurs to satisfy stability criteria that require (i) $\partial \rho / \partial z \geq 0$ for static stability; (ii) $R_b \geq 0.65$ for mixed layer stability; and (iii)

$$R_g = g \frac{\partial \rho / \partial z}{\rho_0 (\partial v / \partial z)^2} \geq 0.25$$

for vertical shear flow stability, where $z = 0$ at the surface and increases downward and R_g is the gradient Richardson number. Given that the original Price et al. (1986) model cannot be implemented in MICOM, the modified version of Chen et al. (1994) was used. This modified version was used to calculate the fraction of TKE production by vertical shear instability E_2 , which has to be removed from the velocity profile to keep a stable velocity structure. This fraction is given by $R = (R_c / R_g)^{1/2} - 1$, where R_c is the critical limit of the Richardson number and R_g is evaluated between two contiguous isopycnic layers. As in Chen et al. (1994), the entrainment sources E_1 and E_2 are merged in a hybrid model ($E_1 + E_2$) that yields an exact expression for the number of isopycnic layers the OML will entrain before the finite energy supply $E = E_1 + E_2$ is exhausted. Standard entrainment/detrainment algorithms of MICOM (Bleck et al. 1989) are used to adjust the OML thickness and density in terms of the total E source. These standard entrainment/detrainment algorithms take care of the static stability criteria and of the thickness of isopycnal layers below the OML.

The model components E_1 and E_2 in Eq. (7) are named Kraus–Turner (KT) and Price–Weller–Pinkel (PWP), respectively. Two general cases are investigated here:

(i) instantaneous wind erosion only (KT) and (ii) vertical entrainment caused simultaneously by KT and shear-driven mixing (KT+PWP). Two stability criteria are used: $R_c = [1, 0.65]$ (Table 2).

b. Wind erosion during the forced stage

Compared with cases that consider upwelling only, KT produced additional OML deepening from about 20 to 25 m in WCE1 and from 10 to 15 m in CCE2 (Fig. 7). Cooling associated with this OML deepening is about 0.3°, 1.5°, and 3°C in WCE1, EFO, and CCE2, respectively (Fig. 8). OML cooling of less than 0.5°C, together with significant layer deepening of about 25 m, indicates that most wind erosion in WCE1 takes place over a nearly homogeneous and deep warm water column. Weak stratification at the OML base of this warm feature (Table 3) facilitates wind erosion.

c. Shear-driven entrainment

The incorporation of TKE production by vertical shear (KT+PWP with critical limits of $R_b = R_g = 1$ in PWP) reproduced additional average OML cooling of about 0.1°C on the right side of the storm track inside WCE1 (Figs. 9a,c). Maximum cooling of about 0.7°C was reproduced by KT+PWP in the vicinity of the moorings, compared with maximum cooling of $\sim 0.5^\circ\text{C}$ by KT. The small difference between KT and KT+PWP indicates that, in this warm anticyclone, most of the cooling was driven by instantaneous wind erosion and near-inertial vertical shear was not an important cooling mechanism, in accord with observational evidence presented elsewhere (Shay and Uhlhorn 2008; JS09; JS10). In the case of CCE2, PWP caused additional cooling of more than 1.2°C that confirms the importance of near-inertial vertical shears for OML cooling in this oceanic cyclone (Figs. 9b,d). Inside CCE2, near-inertial vertical shear instability impacted both the magnitude of the cooling and the horizontal extension of the region of cooling.

5. Near-inertial velocity response

Given the importance of near-inertial wave kinematics for the OML thermal response (JS10), we now investigate the near-inertial velocity response in QG vortices.

a. Decay of OML near-inertial currents

During the first half of the IP, near-inertial OML currents in WCE1 and EFO experiments are nearly in phase (Fig. 10a). Subsequently, the velocity response becomes subinertial in WCE1 and, after the first 3 IPs, NIOs in this warm feature exhibit a phase lag of $\sim 180^\circ$ with respect to NIOs in the EFO experiment. By contrast, NIOs in CCE2 present a phase lag of $\sim 90^\circ$ with

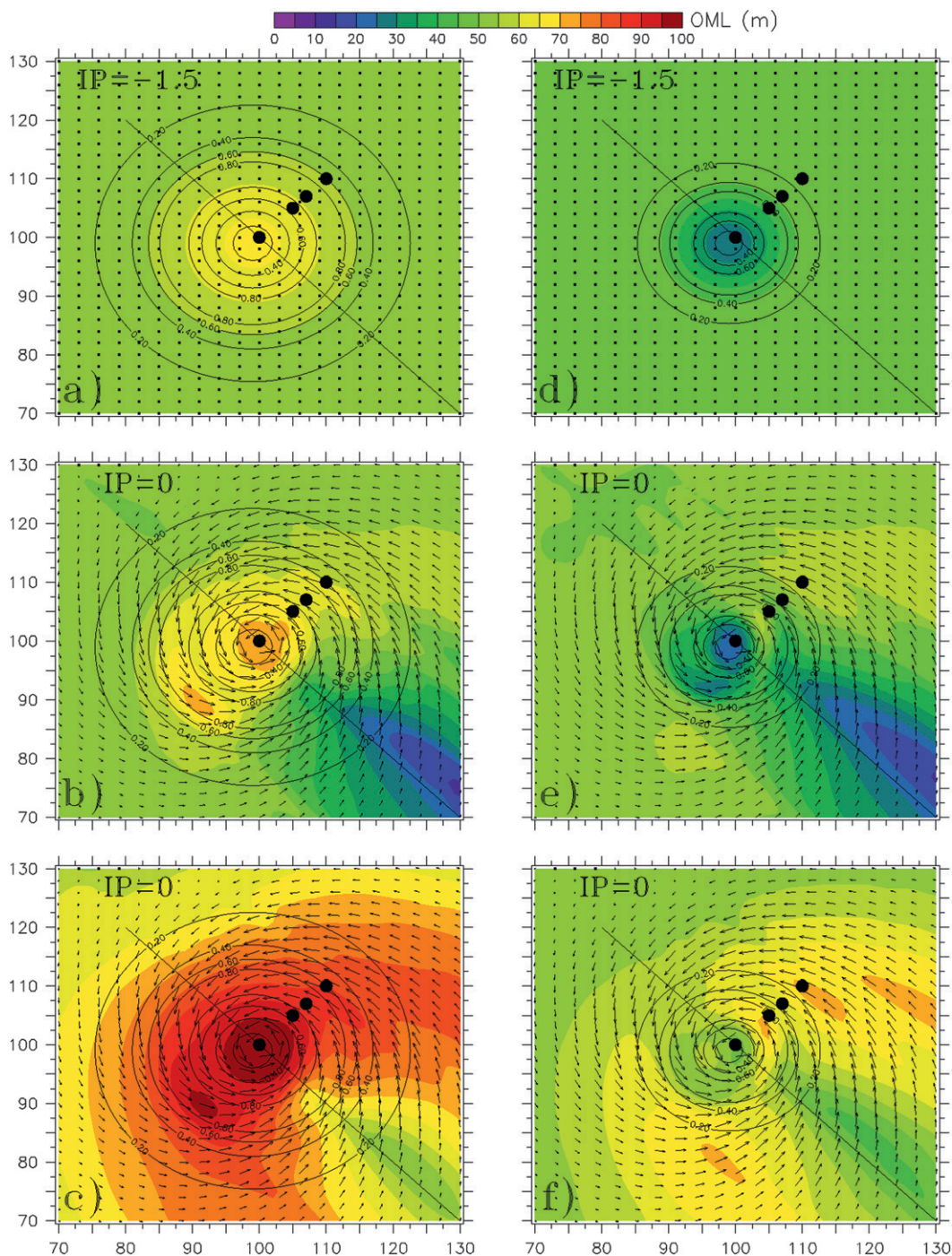


FIG. 7. OML deepening during the forced stage in (a)–(c) WCE1 and (d)–(f) CCE2. (a),(d) Prestorm OML thickness. (b),(e) Change of layer thickness by horizontal current divergence. (c),(f) As in (b),(e), but plus KT. Vectors are for wind stress.

respect to the EFO experiment only after 10 IPs (Fig. 10b). However, the most striking difference is the OML energy decay rate. Compared with EFO conditions, OML near-inertial energy decays much faster in WCE1 and

much slower in CCE2 (Figs. 10a,b). This contrasting energy decay is consistent with observational data (Shay and Uhlhorn 2008; JS09; JS10), theoretical predictions (Kunze 1985), and numerical experiments (Lee and

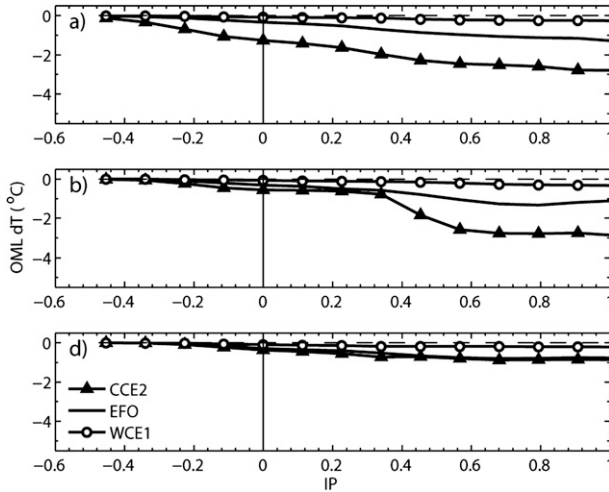


FIG. 8. OML cooling during the forced stage at moorings a, b, and d, using the KT turbulence closure; $dT(IP) = T(IP) - T(IP_0 = -1.5)$ for $IP = -0.5:0.125:1$.

Niiler 1998). Moreover, the OML velocity responses in WCE1 are nearly identical with KT and KT+PWP (Fig. 10a), which indicates that near-inertial vertical shears are not necessarily important for OML energy decay in this warm feature. This result is consistent with observational evidence acquired during TCs Isidore and Lili (Shay and Uhlhorn 2008) and during Katrina and Rita (JS09; JS10). By contrast, near-inertial vertical shear instability (KT+PWP) in CCE2 reduced OML velocity amplitudes by about 40% over the first 6 IP (Fig. 10b).

Gill (1984) ignored turbulence production in the OML and considered the energy decay in the layer as a problem of internal baroclinic mode separation where the relevant time scale is $t_n = 2\pi f / l^2 c_n^2$ (or the time for an 180° phase difference to develop in the OML), $l = 2\pi/\lambda$ is the horizontal wavenumber, λ is the horizontal scale of the wind stress forcing, and c_n is the phase speed of the n th baroclinic mode. In Gill's treatment, the amplitude (sum of individual wave components) of OML near-inertial currents decreases as baroclinic modes become out of phase. The values of c_n and t_n considered in this study (Table 4) qualitatively explain the faster (slower) OML energy decay in WCE1 (CCE1); the EFO experiment has values of c_n and t_n between WCE1 and CCE2 experiments. These predicted values of t_n could be questionable because the definition of t_n is valid for $l c_n / f \ll 1$ (Gill 1984), and this ratio is 1.4, 0.9, and 0.7 for c_1 in WCE1, EFO, and CCE2, respectively.

Note that Gill's definition of t_n only considers the effect of the ocean stratification (via c_n) and neglects the contribution of ζ_g on the decay of OML near-inertial energy. Nevertheless, ζ_g could have an important effect on the horizontal distortion of OML near-inertial

TABLE 3. Stratification characteristics of model QG vortices, with $g' = g(\rho_2 - \rho_1)/\rho_0$. Here, ρ_1 is the initial OML density, ρ_2 is a vertically averaged density from the OML base to a depth of 100 m (approximate depth of the thermocline in CCE2), and ρ_0 is a reference density of 1025 kg m^{-3} .

Vortex	ρ_1 (kg m^{-3})	ρ_2 (kg m^{-3})	ρ_0 (kg m^{-3})	g' (m s^{-2})
CCE2	1024.4	1026.0	1025.0	16×10^{-3}
WCE1	1022.7	1023.7	1025.0	9×10^{-3}

motions, which impacts the vertical structure of the baroclinic modes and the vertical dispersion of near-inertial energy (e.g., Kunze 1985; Young and Ben Jelloul 1997; Lee and Niiler 1998; Danioux et al. 2008). In this study, the OML velocity oscillations in CCEs are at higher frequencies for smaller Ro. For example, after 10 IPs, there is a phase difference of about 45° between the leading NIOs inside CCE1 ($Ro = 0.06$) and those inside CCE2 ($Ro = 0.08$) (Fig. 10d). Given that stratification and the vortex's horizontal scale are the same in these cyclones, this result indicates that the rotational rate of the QG vortex impacts the near-inertial wave frequency response in OMLs (and so vertical dispersion of near-inertial energy into the thermocline). This result is consistent with analytical predictions that show that geostrophic kinetic energy changes the dispersive properties of NIOs (Young and Ben Jelloul 1997). Similarly, in the case of the WCEs, the OML NIOs are shifted toward higher frequencies for smaller Ro. NIOs inside WCE1 ($Ro = 0.06$) lead the velocity response and, after 6 IPs, there is a large phase difference of about 180° with respect to WCE2 ($Ro = 0.08$) (Fig. 10c). This difference in the near-inertial response between WCEs could also be a consequence of the horizontal scale being smaller in the experiment with smaller Ro (WCE1).

b. Vertical structure of near-inertial currents

Given that variations in the Brunt–Väisälä frequency cause an internal NIO to change its amplitude and its vertical wavelength as it propagates vertically through the water column, it is convenient to normalize each velocity profile by using a time mean Brunt–Väisälä frequency $\bar{N}(z)$ at the moorings (Leaman and Sanford 1975). This type of normalization is equivalent to the usual Wentzel–Kramers–Brillouin–Jeffreys (WKBJ) approximation; it enables comparison between different stratification environments (WCEs, CCEs, and EFO) and, in this particular case, facilitates the study of the effects of ζ_g on the near-inertial response through the water column because buoyant effects are isolated. WKBJ-scaled velocities are presented in Fig. 11 (see JS10 for a description of the normalization method). One of the more salient aspects is the downward propagation of the NIO

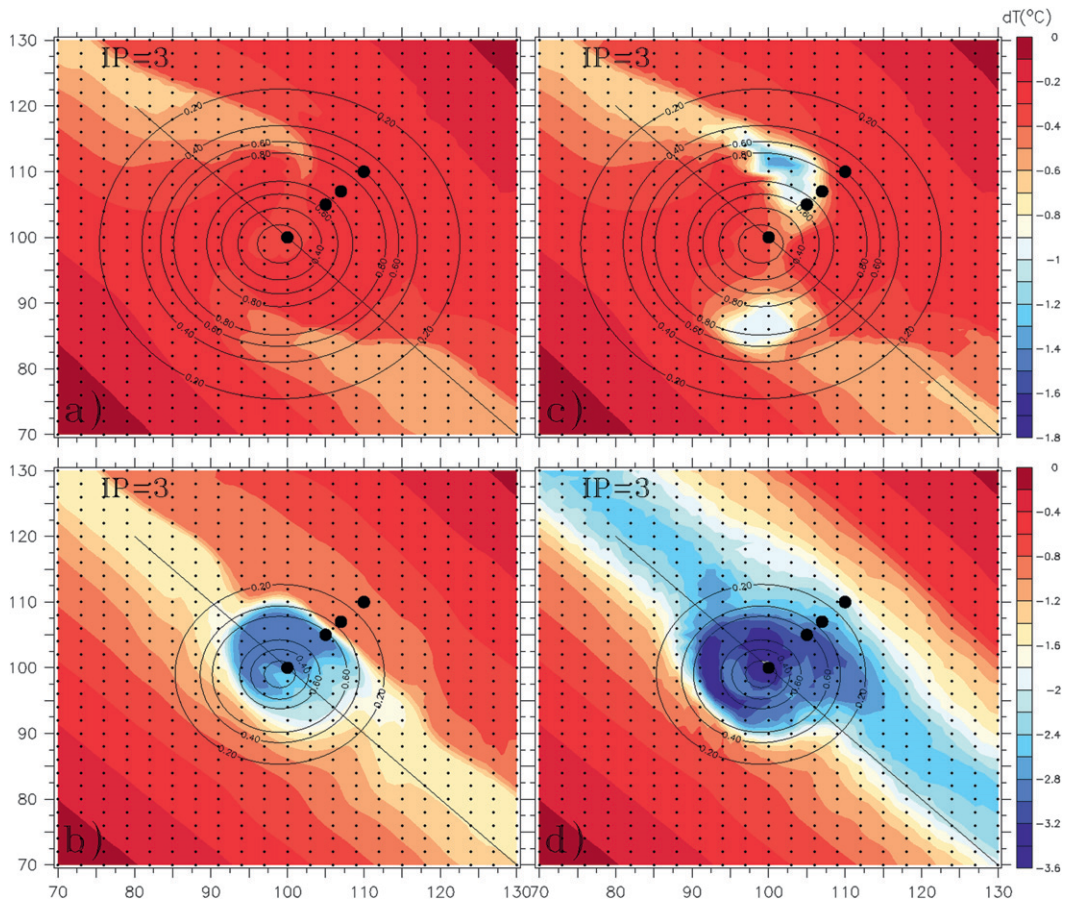


FIG. 9. OML cooling dT in (top) WCE1 and (bottom) CCE2, in terms of (a),(b) the KT turbulence closure and (c),(d) KT+PWP, where $dT = T(\text{IP} = 3) - T(\text{IP} = -1.5)$. Notice the difference in temperature scale between (top) and (bottom).

beams inside WCEs (Figs. 11a,b). This characteristic, together with rapid OML near-inertial energy decay (Fig. 10), confirms that in these anticyclones a larger amount of the kinetic energy injected by TCs propagates downward out of the surface mixed layer. By contrast, fewer NIO beams are present below OMLs in CCEs (Figs. 11c,d) because near-inertial energy is trapped in upper layers, where it increases mixing and entrainment (Fig. 10). This contrasting wave vertical dispersion is in agreement with observational evidence acquired during Katrina and Rita (JS09; JS10).

Inside WCEs, surface and bottom currents are 180° out of phase during the first 5 IPs (Figs. 11a,b), which is consistent with the velocity structure of the first forced baroclinic mode. The velocity inflection point is located at about 600-sm (stretched meters) depth, which suggests that the vertical length of this mode is ~ 1200 sm (or the approximate vertical length of WCEs in the present treatment). Motion at the bottom is possible as soon as the forcing is turned on, presumably caused by

reflection of the first mode structure (Gill 1984; Kundu and Thomson 1985). Both in WCE1 ($Ro = 0.06$) and WCE2 ($Ro = 0.08$), the velocity field below the OML is affected by the first baroclinic mode even during the first IP, in agreement with the predicted time $t_1 = 0.5$ IP (Table 4). CCEs also exhibit velocity structures consistent with the first forced baroclinic mode that prevails during the first 15 IP (Figs. 11c,d). In this case, the change of current direction occurs at ~ 300 -sm depth, corresponding to a vertical scale of about 600 sm for the first mode. The first baroclinic mode structure is apparent since the first half of the first IP, in both CCE1 and CCE2; this time scale is shorter than the predicted value $t_1 = 2.3$ IP (Table 4). Again, given that the vortex's horizontal scale and stratification are the same in these cyclones, only the different Ro causes the differing baroclinic velocity structure between CCE1 and CCE2.

The conventional thought is that vertical dispersion of OML near-inertial energy is governed by separation in the near-inertial modes and that this mode separation is

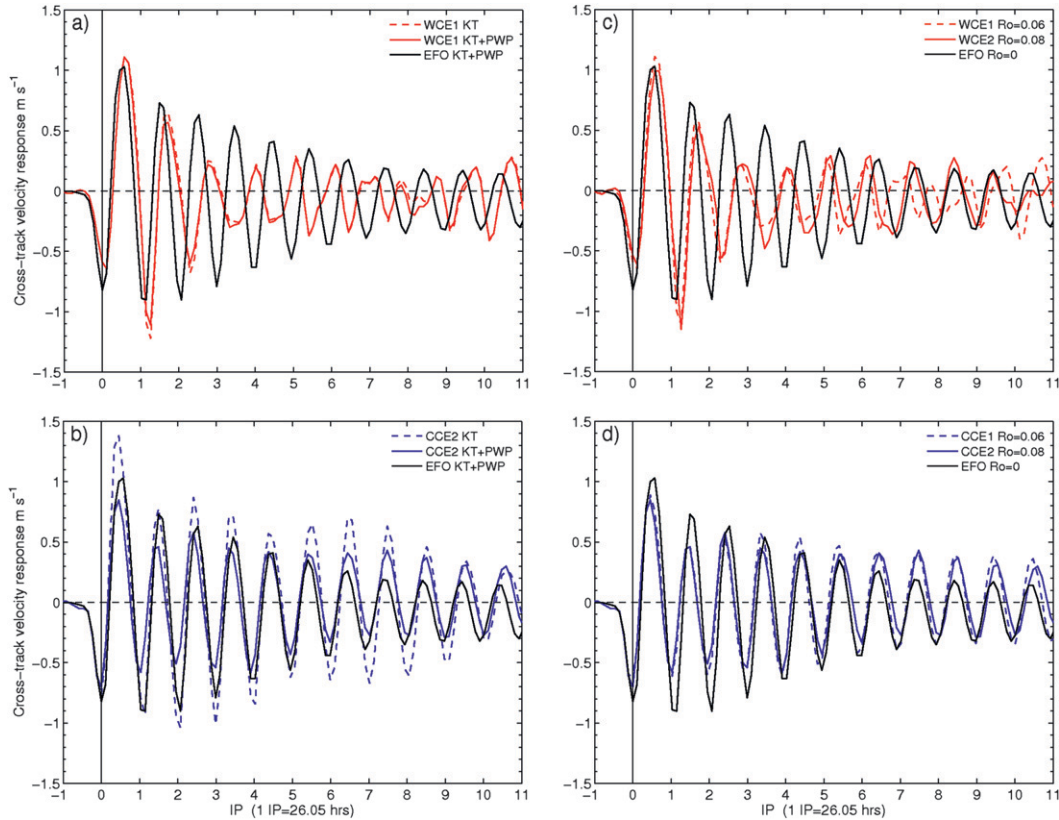


FIG. 10. OML near-inertial velocity response at mooring b. (a),(b) Sensitivity to the turbulence closure for the OML. (c),(d) Sensitivity to Ro.

a function of the horizontal scale of the wind forcing (Gill 1984). Here, however, near-inertial mode separation is also a function of Ro. This result is in agreement with theoretical developments showing that geostrophic kinetic energy K_g causes a rapid loss of phase coherence between near-inertial vertical modes, which greatly increases the vertical propagation of these motions (Young and Ben Jelloul 1997). In Young and Ben Jelloul’s (1997) treatment, the dispersion of NIOs is governed by $\omega_n = (1/2)c_n^2 f(k^2 + l^2) - K_g / fc_n^2$. In this context, a more rapid vertical dispersion of near-inertial motions is predicted as K_g is increased at higher Ro.

Mode separation is more evident in WCEs, as the number of velocity inflection points increases with time because of dispersion of higher modes. From 10 to 15 IPs and for each IP, the current structure inside WCE1 (Ro = 0.06) exhibits two flow reversals with depth that suggest a velocity structure consistent with the second baroclinic mode (Fig. 11a). In the more rapidly rotating WCE2 (Ro = 0.08), the second mode separates faster even when the vortex’s horizontal scale is larger (Fig. 11b). Moreover, higher modes (not present in WCE1 during the first 15 IPs) dominate near-inertial wave activity in WCE2

after 10 IPs. This result suggests that separation in the modes increases with Ro, in accord with Young and Ben Jelloul (1997). By contrast, only the first mode is noticeable in CCEs; this mode is more energetic in CCE2 (Figs. 11c,d).

In short, as NIOs rotate clockwise in the Northern Hemisphere while CCEs rotate anticlockwise, only the more energetic vertical near-inertial modes can overcome the counterrotating background flow in QG cyclones. By

TABLE 4. Phase speed of the first three internal baroclinic modes c_n and time $t_n = 2\pi f / l^2 c_n^2$ for an 180° phase difference to develop in the OML (Gill 1984), where $f(27^\circ\text{N}) = 6.621 \times 10^{-5} \text{ s}^{-1}$; $l = 2\pi/\lambda$; and $\lambda = 168 \text{ km}$ based on the horizontal scale of the wind stress curl, which is assumed to be $\lambda = 4R_{\text{max}}$, with $R_{\text{max}} = 42 \text{ km}$. This scale of λ is comparable to the horizontal scale of CCE2 (150 km) but smaller than the horizontal scale of WCE1 (250 km).

n	WCE1		EFO		CCE2	
	c_n (m s ⁻¹)	t_n (IP)	c_n (m s ⁻¹)	t_n (IP)	c_n (m s ⁻¹)	t_n (IP)
1	2.47	0.5	1.60	1.2	1.17	2.3
2	1.21	2.1	0.90	3.9	0.68	6.9
3	0.73	5.9	0.56	10.1	0.42	18.0

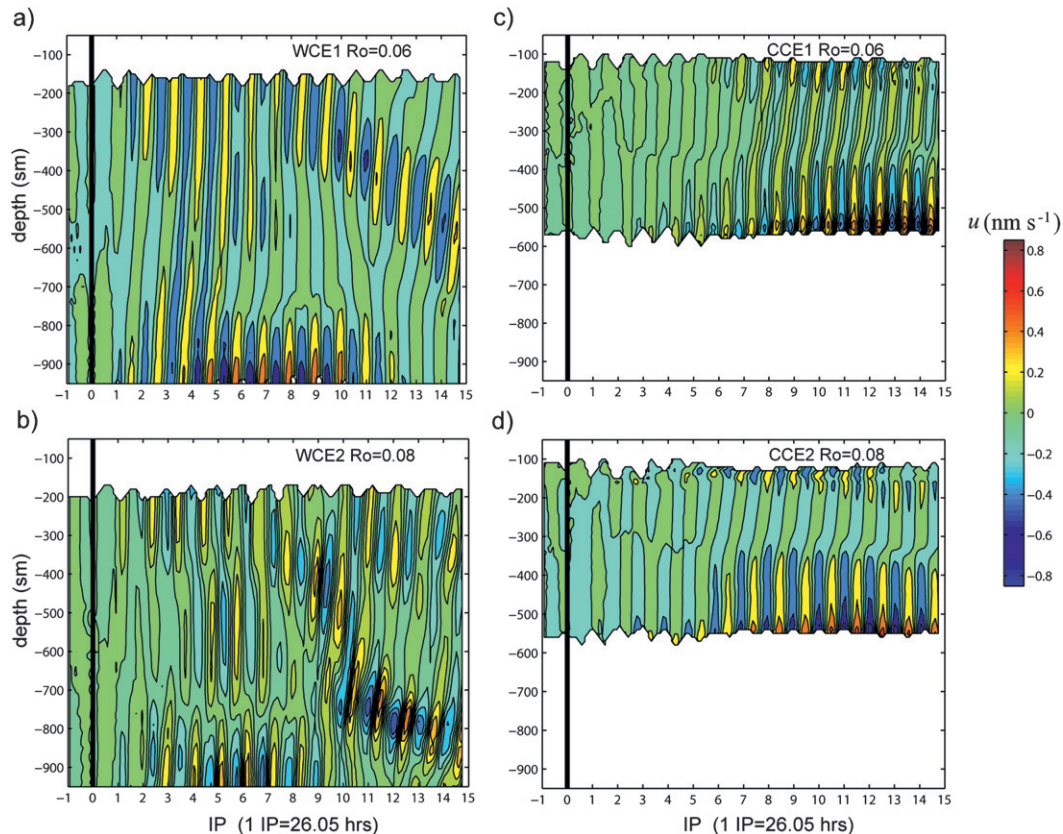


FIG. 11. WKBJ-scaled cross-track velocity u at mooring b (KT+PWP closure); the units of u are normalized m s^{-1} (see text for details). Note that depth is stretched [units in stretched meters (sm)]. These velocity fields are interpolated into a regular vertical grid. The bold vertical line represents the passage of the storm's eye over the vortex's center.

contrast, the corotation of NIOs and WCEs should facilitate vertical dispersion of near-inertial energy in QG anticyclones. Moreover, the presence of baroclinic modal structures inside QG vortices suggests that, rather than the vertical scale of the full water column, the vortex's vertical length determines the vertical scales and structure of forced modes.

6. Discussion

a. Critical layer in CCEs

NIOs forced by Katrina in a Gulf of Mexico's CCE produced a critical layer that extended between the 100- and 150-m-depth levels (JS10). Given that amplification of near-inertial kinetic energy over this water column produced important vertical shear and mixing events, it is of interest to know whether KT and PWP at different Ro can reproduce this critical layer. In this context, vertical distributions of time-averaged perturbation kinetic energy $\overline{K'}$ are computed from the numerical experiments. Perturbation velocities were obtained by removing

vertical and time averages from 8 to 11 IPs. Perturbation kinetic energies K' were then calculated from these perturbation velocities at 3-h intervals (time span of model outputs). Finally, K' was time averaged from 8 to 11 IPs as in JS10.

The KT model alone does not reproduce the observed layer of maximum K' (subsurface critical layer; JS10) below the OML, in neither CCE1 ($Ro = 0.06$) nor CCE2 ($Ro = 0.08$) (Fig. 12). By incorporating TKE production by vertical shear instability over the stratified ocean, higher values of K' are attained in CCE1 (Fig. 12a). However, PWP reproduced more realistic values of K' at higher Ro (CCE2), particularly at lower values of the critical limit of the gradient Richardson number (Fig. 12b). There is more vertical shear instability in CCE2 because the near-inertial response is more energetic (Figs. 11c,d); that is, the more energetic QG cyclones are more efficient near-inertial mixers of the upper ocean. The KT experiments reproduced higher energy levels than KT+PWP at deep waters (below the 200-m-depth level), in both CCE1 and CCE2. This result is a consequence of the KT model

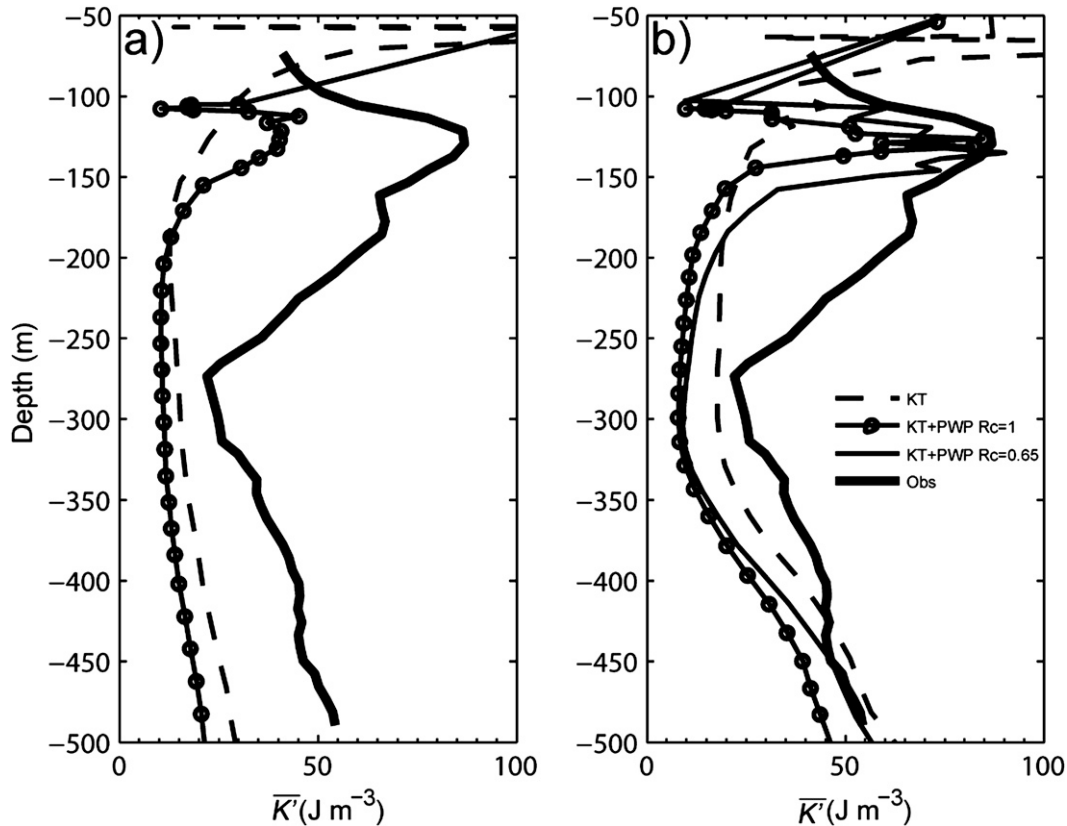


FIG. 12. Vertical distribution of time-averaged (from 8 to 11 IP) perturbation kinetic energy $\overline{K'}$ at mooring b: (a) CCE1 ($Ro = 0.06$) and (b) CCE2 ($Ro = 0.08$). Bold lines are from direct measurements inside the CCE that interacted with Katrina (JS10). Here, R_c is the critical limit of bulk and gradient Richardson numbers.

not mixing over the stratified ocean below the OML; hence, more perturbation kinetic energy propagates downward. To reproduce critical layers similar to that triggered by Katrina, numerical models have to represent vertical shear instability and mixing over the thermocline.

b. Trapped cold wake

Under quiescent ocean conditions, the cold wake of a TC is typically observable on the right side of its track during several weeks after its passage and over a distance of $O(10^3)$ km. However, several days after the passages of TCs Hilda (Leipper 1967), Ivan (Walker et al. 2005; Halliwell et al. 2008, 2011), and Katrina (JS10) over CCEs in the eastern Gulf of Mexico, the region of maximum TC-induced OML cooling was observed to the left of the storm track, which suggests that these cold temperature anomalies were advected westward by propagating CCEs. To evaluate this idea, two numerical experiments were conducted, one for CCE1 and another for CCE2, in which the β plane is turned on at IP = 1, or a few hours after the direct TC–CCE interaction. There are two corresponding f -plane experiments to compare

with (Table 2). To evaluate the effects of the TC wind stress on the propagation speed of CCE2, another β -plane experiment was conducted for this vortex in absence of wind forcing.

In the case of f -plane experiments, the region of maximum TC-induced OML cooling remained stationary with the CCE during the first 15 IPs (Figs. 13a,c). That is, the TC wind stress did not move the CCE from its original position, which is not surprising, given the fast translation speed of the storm (6.3 m s^{-1}). By contrast, in β -plane experiments, the CCE drifted northwestward about 100 km from its original position during the first 15 IPs, and it carried the TC-induced temperature anomaly with an average speed of roughly 6 km day^{-1} (Figs. 13b,d). The position of CCE2 at IP = 15 is basically the same for both the wind-forced and nonwind-forced β -plane experiments. Thus, in the case of a fast moving storm, the impulsive wind stress did not have an important impact on the propagation speed of CCE2.

Another possibility is that the cold wake patch that was observed on the left side of the real Katrina's track was caused by the presence of a prestorm CCE that

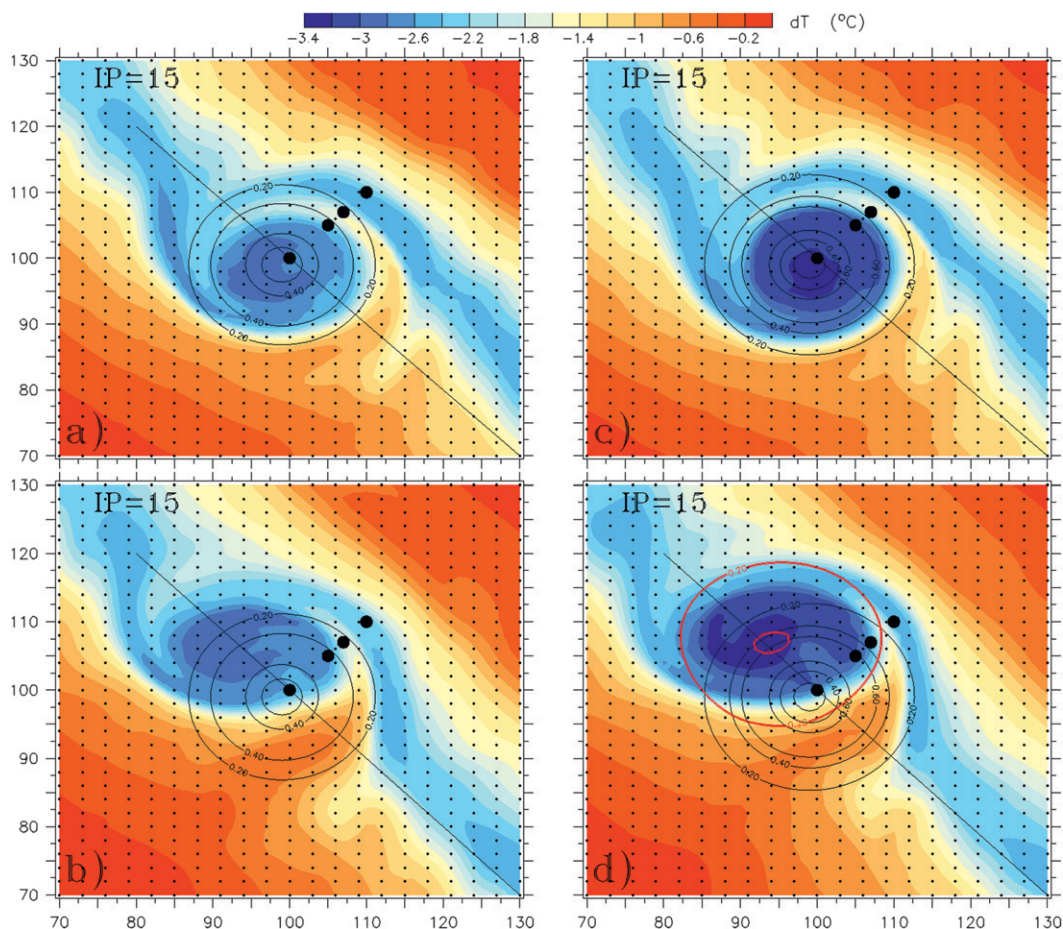


FIG. 13. TC-induced OML cooling dT in CCEs in (top) the f plane and (bottom) the β plane, where $dT = T(\text{IP} = 15) - T(\text{IP} = -1.5)$ and the OML turbulence closure is KT+PWP: (a),(b) CCE1 ($\text{Ro} = 0.06$) and (c),(d) CCE2 ($\text{Ro} = 0.08$). Circular black contours are the magnitude of OML currents at $t = -1.5$ IP (initial conditions). Red contours in (d) are the magnitude of OML currents at $t = 15$ IP for CCE2 in the β plane, in absence of wind forcing.

extended to the west of the storm's track (at 28°N , 90°W in Fig. 1b of JS10). To explore this idea, the original storm track was shifted 1° to the east of the CCE2's center in an f -plane experiment. As shown in Fig. 14, in this case the TC produced OML cooling between 1° and 1.5°C in CCE2; this vortex was mostly influenced by wind forcing at tropical storm intensity level.

7. Summary and concluding remarks

Thermal and near-inertial velocity responses of QG vortices to TC forcing were investigated in an isopycnic ocean model, for both cyclones and anticyclones and for Ro numbers representative of geostrophic features that interacted with TCs Katrina and Rita in the Gulf of Mexico. A turbulence closure for the OML was used that considers (i) instantaneous wind erosion by the wind-driven OML frictional velocity (KT closure) and (ii) TKE

production by vertical shear instability at the OML base and over the stratified ocean underneath (modified PWP closure).

During the forced stage (first half of the inertial period), wind-driven horizontal current divergence is also a function of underlying geostrophic relative vorticity as well as the wind stress curl. For the same wind stress curl forcing, independent of the angle of approach of the storm to the QG vortex, upwelling (downwelling) regimes predominantly develop under the storm's eye when the wind stress vector is with (against) the geostrophic OML velocity vector. Rather than just a function of the wind stress curl itself, upwelling/downwelling velocities are a function of the curl of wind-driven acceleration of OML geostrophic currents. This curl emerges where the initial OML thickness is not uniform (as in WCEs and CCEs); differential advection of geostrophic vorticity by the wind stress is the mechanism that creates this curl. This

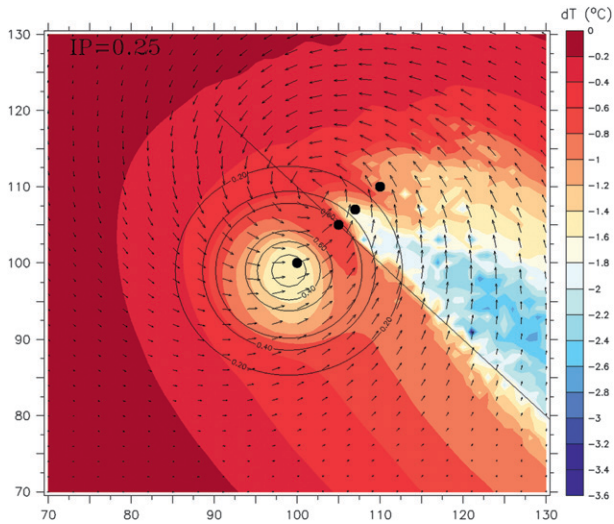


FIG. 14. TC-induced OML cooling dT in CCE2 ($Ro = 0.08$) in the f plane, where $dT = T(IP = 0.25) - T(IP = -1.5)$ and the OML turbulence closure is KT+PWP. Circular black contours are the magnitude of OML currents at $t = -1.5$ IP (initial conditions). The storm track is shifted 1° to the east with respect to the vortex's center. Vectors are for the wind stress.

result is consistent with observational data (JS09), theoretical predictions (Stern 1965), and more realistic numerical experiments (Halliwell et al. 2008).

Instantaneous wind erosion produced most OML cooling in WCEs. Reduced cooling of less than 1°C in these warm features results because turbulent mixing takes place over a warm, deep, and nearly homogeneous surface water column and because near-inertial shears do not develop as OML near-inertial energy is rapidly dispersed into the thermocline. This result underscores the importance of the oceanic heat content (relative to the 26°C isotherm depth) for possible feedback mechanisms to storm intensity over warm oceanic features. In CCEs, upwelling of cold water and instantaneous wind stirring produced OML cooling of about 2.2°C during the forced stage, and near-inertial shear-driven entrainment produced additional OML cooling of about 1.6°C during the relaxation stage. Considering TKE production by vertical shear instability and higher vertical resolution over the stratified ocean below the OML reproduced more realistic TC-induced cooling levels. Modeled cooling levels were consistent with observed OML cooling induced by TCs Katrina and Rita over geostrophic oceanic eddies (JS09; JS10).

Background geostrophic relative vorticity clearly modulates vertical dispersion of OML near-inertial energy. The near-inertial velocity response is shifted toward more subinertial and energetic frequencies inside WCEs, where rapid vertical dispersion prevents accumulation of kinetic

energy and momentum in the upper ocean, thereby reducing vertical shear development and entrainment at the layer base. By contrast, near-inertial oscillations are dampened in OMLs of CCEs, which enhances vertical shear and mixing at the layer base. This contrasting dispersion of near-inertial energy is consistent with observational evidence acquired during Katrina and Rita (JS10), theoretical developments (Kunze 1985; Young and Ben Jelloul 1997), and numerical experiments (Lee and Niiler 1998; Danioux et al. 2008). Numerical models that neglect geostrophic features can significantly underestimate or overestimate OML cooling, because they fail to accurately represent OML near-inertial energy decay, which affects the amount of kinetic energy available for vertical entrainment at the layer base.

Rotational and translation characteristics of QG vortices have an important impact on the tridimensional structure of near-inertial wave wakes produced by TCs. As Ro increases, the near-inertial response is more energetic and strengthens vertical shears and mixing in both CCEs and WCEs. The rotational rate and vertical length of the QG vortex (rather than the full depth of the water column) presumably determine the vertical structure of forced baroclinic modes. Observed characteristics of the wake of Katrina inside a CCE (JS10), such as the critical layer and vertical structure of near-inertial currents, were better reproduced at higher Ro . Moreover, the temperature anomaly caused by TCs in QG vortices is carried away westward with time. This process, together with the presence of QG vortices on the west side of the TC's tracks, produce important cold wake patches on the left side of the track. Numerical models used to investigate the effects of TCs on climate that do not resolve geostrophic oceanic eddies will not reproduce this patchiness and trapping of the cold wake by geostrophic vortices. Therefore, they will not reproduce feedback mechanisms to atmospheric processes in the right place. This can be a critical issue over western boundary currents and their meanders and geostrophic vortices.

The presence of geostrophic features clearly impacts the contribution of wind-induced NIOs to the global internal wave power and vertical mixing below the OML: WCEs are efficient near-inertial chimneys (Lee and Niiler 1998) and CCEs are efficient near-inertial mixers of the upper ocean. Recent estimates indicate that nearly 70% of the wind-induced near-inertial energy is not available to generate diapycnal mixing at great depth, because this amount of energy is lost to turbulent mixing over the top 200 m (Zhai et al. 2009), in agreement with the case of CCEs presented here and observational evidence acquired during TCs Katrina and Rita (JS09; JS10). More research is needed to assess the role of

geostrophic ocean features in modulating the contribution of wind-induced near-inertial energy to the global meridional overturning circulation.

In conclusion, for models to realistically reproduce TC-induced OML cooling, near-inertial energy dispersion, and feedback mechanisms to storm intensity and atmospheric processes, they should (i) accurately resolve the stratified ocean between the OML base and the thermocline; (ii) yield TKE production by vertical shear instability over the stratified ocean below the OML; and (iii) be initialized with a fair representation of geostrophic features, including position, and velocity, thermal, and density structures.

Acknowledgments. The research team gratefully acknowledges support from the NSF (ATM-04-44525); NASA Hurricane Science Program (NASA Award NNX09AC47G); NOAA Joint Hurricane Testbed program (NOAA Grant NA17RJ1226); NOAA NESDIS; and the Department of the Interior's Bureau of Ocean Energy Management, Regulation and Enforcement (BOEMRE) Dynamics of the Loop Current Study (BOEMRE Contract M08PC20052). The project continues to be grateful to the NOAA Aircraft Operation Center (Dr. Jim McFadden), which makes it possible to acquire high quality data during hurricanes through the Hurricane Forecast Improvement Project (HFIP), and the collaborative ties with NOAA's Hurricane Research Division directed by Dr. Frank Marks at AOML and NOAA's Environmental Modeling Center directed by Dr. Hendrick Tolman at NCEP. Dr. Laurent Chérubin (UM/RSMAS) provided an early version of the modified MICOM code and insightful discussions on the analytical model used to initialize model vortices. Dr. Sang-Ki Lee (NOAA/AOML) kindly facilitated the modified version of the PWP code. Valuable comments and suggestions from three anonymous reviewers helped to clarify and improve this paper. Altimeter products were produced by Ssalto/Duacs and distributed by AVISO, with support from CNES (<http://www.aviso.oceanobs.com/duacs/>).

REFERENCES

- Bleck, R., and E. P. Chassignet, 1994: Simulating the oceanic circulation with isopycnic-coordinate models. *The Oceans: Physical-Chemical Dynamics and Human Impact*, S. K. Majumdar et al., Eds., The Pennsylvania Academy of Science, 17–39.
- , H. P. Hanson, D. Hu, and E. B. Kraus, 1989: Mixed layer-thermocline interaction in a three-dimensional isopycnic coordinate model. *J. Phys. Oceanogr.*, **19**, 1417–1439.
- Carton, X. J., and B. Legras, 1994: The life-cycle of tripoles in 2D incompressible flows. *J. Fluid Mech.*, **267**, 53–82.
- Chang, S., and R. Anthes, 1978: Numerical simulations of the ocean's nonlinear baroclinic response to translating hurricanes. *J. Phys. Oceanogr.*, **8**, 468–480.
- Chen, D., L. M. Rothstein, and A. J. Busalacchi, 1994: A hybrid vertical mixing scheme and its application to tropical ocean models. *J. Phys. Oceanogr.*, **24**, 2156–2179.
- Chérubin, L. M., Y. Morel, and E. P. Chassignet, 2006: Loop Current ring shedding: The formation of cyclones and the effect of topography. *J. Phys. Oceanogr.*, **36**, 569–591.
- Danioux, E., P. Klein, and P. Rivière, 2008: Propagation of wind energy into the deep ocean through a fully turbulent mesoscale eddy field. *J. Phys. Oceanogr.*, **38**, 2224–2241.
- Donelan, M. A., B. K. Haus, N. Reul, W. J. Plant, M. Stiassnie, H. C. Graber, O. B. Brown, and E. S. Saltzman, 2004: On the limiting aerodynamic roughness of the ocean in very strong winds. *Geophys. Res. Lett.*, **31**, L18306, doi:10.1029/2004GL019460.
- Elliot, B. A., 1982: Anticyclonic rings in the Gulf of Mexico. *J. Phys. Oceanogr.*, **12**, 1292–1309.
- Flierl, G. R., 1987: Isolated eddy models in geophysics. *Annu. Rev. Fluid Mech.*, **19**, 493–530.
- French, J. R., W. M. Drennan, J. A. Zhang, and P. G. Black, 2007: Turbulent fluxes in the hurricane boundary layer. Part I: Momentum flux. *J. Atmos. Sci.*, **64**, 1089–1102.
- Gill, A. E., 1984: On the behavior of internal waves in the wake of storms. *J. Phys. Oceanogr.*, **14**, 1129–1151.
- Greatbatch, R. J., 1984: On the response of the ocean to a moving storm: Parameters and scales. *J. Phys. Oceanogr.*, **14**, 59–78.
- Griffies, S. M., R. C. Pacanowski, and R. W. Hallberg, 2000: Spurious diapycnal mixing associated with advection in a z-coordinate ocean model. *Mon. Wea. Rev.*, **128**, 538–564.
- Halliwell, G. R., L. K. Shay, S. D. Jacob, O. M. Smedstad, and E. W. Uhlhorn, 2008: Improving ocean model initialization for coupled tropical cyclone forecast models using GODAE nowcasts. *Mon. Wea. Rev.*, **136**, 2576–2591.
- , —, J. K. Brewster, and W. J. Teague, 2011: Evaluation and sensitivity analysis of an ocean model to Hurricane Ivan. *Mon. Wea. Rev.*, **139**, 921–945.
- Hamilton, P., 1992: Lower continental slope cyclonic eddies in the central Gulf of Mexico. *J. Geophys. Res.*, **97** (C2), 2185–2200.
- Herbette, S., Y. Morel, and M. Arhan, 2003: Erosion of a surface vortex by a seamount. *J. Phys. Oceanogr.*, **33**, 1664–1679.
- Hong, X., S. W. Chang, S. Raman, L. K. Shay, and R. Hodur, 2000: The interaction between Hurricane Opal (1995) and a warm core ring in the Gulf of Mexico. *Mon. Wea. Rev.*, **128**, 1347–1365.
- Jacob, S. D., and L. K. Shay, 2003: The role of mesoscale features on the tropical cyclone-induced mixed layer response: A case study. *J. Phys. Oceanogr.*, **33**, 649–676.
- , —, A. J. Mariano, and P. G. Black, 2000: The 3D mixed layer response to Hurricane Gilbert. *J. Phys. Oceanogr.*, **30**, 1407–1429.
- Jaimes, B., 2009: On the response to tropical cyclones in mesoscale oceanic eddies. Ph.D. dissertation, University of Miami, 145 pp.
- , and L. K. Shay, 2009: Mixed layer cooling in mesoscale oceanic eddies during Hurricanes Katrina and Rita. *Mon. Wea. Rev.*, **137**, 4188–4207.
- , and —, 2010: Near-inertial wave wake of Hurricanes Katrina and Rita over mesoscale oceanic eddies. *J. Phys. Oceanogr.*, **40**, 1320–1337.
- Kraus, E. B., and J. S. Turner, 1967: A one-dimensional model of the seasonal thermocline. II: The general theory and its consequences. *Tellus*, **19**, 98–105.

- Kundu, P. K., and R. E. Thomson, 1985: Inertial oscillations due to a moving front. *J. Phys. Oceanogr.*, **15**, 1076–1084.
- Kunze, E., 1985: Near-inertial wave propagation in geostrophic shear. *J. Phys. Oceanogr.*, **15**, 544–565.
- Large, W. G., and S. Pond, 1981: Open ocean momentum flux measurements in moderate to strong wind. *J. Phys. Oceanogr.*, **11**, 324–336.
- Leaman, K., and T. Sanford, 1975: Vertical energy propagation of inertial waves: A vector spectral analysis of velocity profiles. *J. Geophys. Res.*, **80**, 1975–1978.
- Lee, D.-K., and P. P. Niiler, 1998: The inertial chimney: The near-inertial energy drainage from the ocean surface to the deep layer. *J. Geophys. Res.*, **103** (C4), 7579–7591.
- Leipper, D. F., 1967: Observed ocean conditions and Hurricane Hilda, 1964. *J. Atmos. Sci.*, **24**, 182–186.
- Lin, I.-I., C.-C. Wu, K. A. Emanuel, I.-H. Lee, C.-R. Wu, and I.-F. Pun, 2005: The interaction of Supertyphoon Maemi (2003) with a warm ocean eddy. *Mon. Wea. Rev.*, **133**, 2635–2649.
- Morel, Y., and J. McWilliams, 2001: Effects of isopycnal and diapycnal mixing on the stability of oceanic currents. *J. Phys. Oceanogr.*, **31**, 2280–2296.
- , and L. N. Thomas, 2009: Ekman drift and vortical structures. *Ocean Modell.*, **27**, 185–197.
- , D. S. Darr, and C. Talandier, 2006: Possible sources driving the potential vorticity structure and long-wave instability of coastal upwelling and downwelling currents. *J. Phys. Oceanogr.*, **36**, 875–896.
- Niiler, P. P., and E. B. Kraus, 1975: One-dimensional models of the upper ocean. *Modelling and Prediction of the Upper Layers of the Ocean*, E. B. Kraus, Ed., Pergamon Press, 143–172.
- O'Brien, J. J., 1967: The non-linear response of a two-layer, baroclinic ocean to a stationary, axially-symmetric hurricane: Part II: Upwelling and mixing induced by momentum transfer. *J. Atmos. Sci.*, **24**, 208–215.
- , and R. O. Reid, 1967: The non-linear response of a two-layer, baroclinic ocean to a stationary, axially-symmetric hurricane: Part I: Upwelling induced by momentum transfer. *J. Atmos. Sci.*, **24**, 197–207.
- Powell, M. D., P. J. Vickery, and T. A. Reinhold, 2003: Reduced drag coefficient for high wind speeds in tropical cyclones. *Nature*, **422**, 279–283.
- Price, J. F., 1981: Upper ocean response to a hurricane. *J. Phys. Oceanogr.*, **11**, 153–175.
- , C. N. K. Mooers, and J. C. Van Leer, 1978: Observation and simulation of storm-induced mixed-layer deepening. *J. Phys. Oceanogr.*, **8**, 582–599.
- , R. A. Weller, and R. Pinkel, 1986: Diurnal cycling: Observations and models of the upper ocean response to diurnal heating, cooling, and wind mixing. *J. Geophys. Res.*, **91** (C7), 8411–8427.
- Rogers, R., and Coauthors, 2006: The Intensity Forecasting Experiment (IFEX): A NOAA multiyear field program for improving tropical cyclone intensity forecasts. *Bull. Amer. Meteor. Soc.*, **87**, 1523–1537.
- Schade, L. R., and K. A. Emanuel, 1999: The ocean's effect on the intensity of tropical cyclones: Results from a simple coupled atmosphere–ocean model. *J. Atmos. Sci.*, **56**, 642–651.
- Shay, L. K., 2009: Upper ocean structure: Response to strong forcing events. *Encyclopedia of Ocean Sciences*, 2nd ed. J. Steele et al., Eds., Elsevier Press International, 4619–4637.
- , and S. D. Jacob, 2006: Relationship between oceanic energy fluxes and surface winds during tropical cyclone passage. *Atmosphere-Ocean Interactions*, W. Perrie, Ed., Advances in Fluid Mechanics, Vol. 2, WIT Press, 115–142.
- , and E. W. Uhlhorn, 2008: Loop Current response to Hurricanes Isidore and Lili. *Mon. Wea. Rev.*, **136**, 3248–3274.
- , R. L. Elsberry, and P. G. Black, 1989: Vertical structure of the ocean current response to a hurricane. *J. Phys. Oceanogr.*, **19**, 649–669.
- , S. W. Chang, and R. L. Elsberry, 1990: Free surface effects on the near-inertial current response to a hurricane. *J. Phys. Oceanogr.*, **20**, 1405–1424.
- , P. G. Black, A. J. Mariano, J. D. Hawkins, and R. L. Elsberry, 1992: Upper ocean response to Hurricane Gilbert. *J. Geophys. Res.*, **97** (C12), 20 227–20 248.
- , G. J. Goni, and P. G. Black, 2000: Effects of a warm oceanic feature on Hurricane Opal. *Mon. Wea. Rev.*, **128**, 1366–1383.
- Stern, M. E., 1965: Interaction of a uniform wind stress with a geostrophic vortex. *Deep-Sea Res.*, **12**, 355–367.
- Vickery, P. J., D. Wadhwa, M. D. Powell, and Y. Chen, 2009: A hurricane boundary layer and wind field model for use in engineering applications. *J. Appl. Meteor. Climatol.*, **48**, 381–405.
- Wada, A., and J. C. L. Chan, 2008: Relationship between typhoon activity and upper ocean heat content. *Geophys. Res. Lett.*, **35**, L17603, doi:10.1029/2008GL035129.
- Walker, N. D., R. R. Leben, and S. Balasubramanian, 2005: Hurricane-forced upwelling and chlorophyll *a* enhancement within cold-core cyclones in the Gulf of Mexico. *Geophys. Res. Lett.*, **32**, L18610, doi:10.1029/2005GL023716.
- Wu, C.-C., C.-Y. Lee, and I.-I. Lin, 2007: The effect of the ocean eddy on tropical cyclone intensity. *J. Atmos. Sci.*, **64**, 3562–3578.
- Young, W. R., and M. Ben Jelloul, 1997: Propagation of near-inertial oscillations through a geostrophic flow. *J. Mar. Res.*, **55**, 735–766.
- Zhai, X., R. J. Greatbatch, C. Eden, and T. Hibiya, 2009: On the loss of wind-induced near-inertial energy to turbulent mixing in the upper ocean. *J. Phys. Oceanogr.*, **39**, 3040–3045.